Double Diffusion in Powell Lake:

New Insights from a Unique Case Study

by

Benjamin Scheifele

B.Sc. Physics, St. Francis Xavier University, 2011

A THESIS SUBMITTED IN PARTIAL FULFILLMENT
OF THE REQUIREMENTS FOR THE DEGREE OF

Master of Science

in

THE FACULTY OF GRADUATE AND POSTDOCTORAL STUDIES
(Oceanography)

THE UNIVERSITY OF BRITISH COLUMBIA
(Vancouver)

September 2013

Abstract

High resolution measurements of temperature and electrical conductivity in Powell Lake, British Columbia provide an extensive set of layer and interface observations of a double diffusive staircase found between 325–350 m depth. Powell Lake is an ex-fjord with a quiescent salt layer at thermal steady state in which double diffusion is naturally isolated from turbulent and advective processes. Layers are coherent on the basin scale and their characteristics have a well defined vertical structure. The steady state heat flux is estimated from the large-scale temperature profile and agrees with an earlier estimate of the flux in the sediments. These estimates are compared to a 4/3 flux parameterization which agrees with the steady state flux to within a factor of 2. The discrepancy is explained by testing the scaling underlying the parameterization directly, and it is found that the assumed power law deviates systematically from the observations. Consequently, a different scaling which better describes the observations is presented. The assumption that interfacial fluxes are dominated by molecular diffusion is tested by comparing the interfacial gradient to that expected from the steady state heat flux; at low density ratios, the average interfacial gradient is not sufficiently large to account for transport by molecular diffusion alone, indicating that double diffusive fluxes cannot generally be estimated from bulk interface properties. Salinity interfaces are only marginally (9%) smaller than temperature interfaces, and a simple model to describe the observed difference is presented and shown to be consistent with the observations.

Preface

This thesis is authored by me, Benjamin Scheifele, and describes original work carried out by me under the supervision of Dr. Richard Pawlowicz. I independently collected and analyzed the data described in Chapters 2 and 3 according to a plan jointly developed with Dr. Pawlowicz. Novel theoretical ideas presented in Chapter 4 are mine; however, the discussion surrounding these ideas was likewise developed in conjunction with Dr. Pawlowicz.

Results are unpublished, but are undergoing preparation for submission. Figure 1.4 in Chapter 1 is reproduced with permission from Kelley et al. (2003).

Table of Contents

List of Tables

List of Figures

Acknowledgments

The work you will read about here bears the marks of many who have helped bring this project together from conception to conclusion. These include those who were directly involved —Chris Payne, Lora Pakhomova, Roger Pieters, Greg Lawrence, Kristin Orians, and Bernard Laval— as much as those who shared my life or my office or my living space and who have helped make the past two years both fun and memorable. I am grateful to all of you.

I also want to extend a special and very heartfelt thank–you to a few people who supported me the whole way and so have shaped my entire experience at UBC into the meaningful one it has become:

- . . . Tara Ivanochko, who has been my mentor, advocate, and friend this year.
- . . . Rich Pawlowicz, who has encouraged me to explore both oceans and mountains.
- . . . my parents, Bernd and Josaphine, who love me and put up with me always.

And always both last and first, I want to thank God, through whom I do everything that I accomplish.

Chapter 1

Introduction

1.1 Double Diffusive Convection

Double diffusive convection, or simply "double diffusion", is a transport process that is observed over vast regions of the world's oceans and in numerous lakes around the world (Carpenter and Timmermans, 2012; Kelley et al., 2003). It is comprised of convective motions that occur because of instabilities that can form during the simultaneous diffusion of salt and heat. Temperature and salinity determine the relative density of seawater, and when these have vertical structures such that one stabilizes the watercolumn while the other is gravitationally unstable, the much higher diffusion rate of heat relative to that of salt is able to release the stored potential gravitational energy in the unstable density component. Thus even in the absence of mechanical mixing, convective motions can be established through the creation of an instability which substantially enhance the transports of heat and salt relative to those which would be supported by molecular diffusion alone.

To a first approximation, the density ρ of a watercolumn can be written as

$$\rho = \rho_0 \left(1 + \alpha T + \beta S\right) \tag{1.1}$$

where ρ_0 is a reference density, T the temperature in °C, and S the salinity in g/kg. The coefficient α is the thermal expansion coefficient which quantifies the density response to changes in temperature. It is defined as

$$\alpha = -\frac{1}{\rho_0}\frac{\partial \rho}{\partial T} \tag{1.2}$$

and is usually positive in oceanographic ranges of temperature and salinity. β is the haline

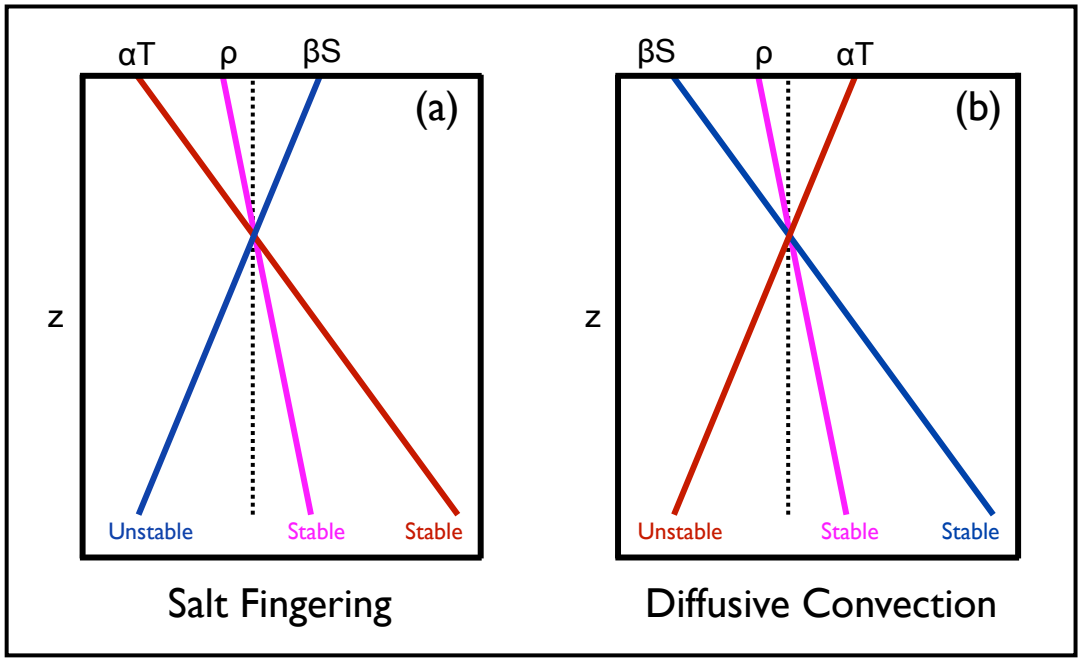

Figure 1.1 – A schematic of two double diffusive background stratifications, leading to two distinct modes of double diffusion. (a) The salt fingering mode occurs when the salinity contribution to the density stratification is unstable, but the temperature stratification is stable. (b) The diffusive layering mode occurs when the opposite is true and salinity provides the stabilizing component while temperature stratification is unstable. In both scenarios, the net density profile is stable.

contraction coefficient defined as

$$\beta = \frac{1}{\rho_0}\frac{\partial \rho}{\partial S} \tag{1.3}$$

which quantifies the density response to changes in salinity and is always positive.

Apart from the constant ρ_0, all variables are in general functions of z, the vertical coordinate which we define positive upwards. From Equation 1.1, there are two ways to set up a stratification that has one stable and one unstable component but a net stratification that is still stable, and these two scenarios lead to two distinct modes of double diffusion (Figure 1.1). Assuming oceanographic ranges and a net stable stratification, if T and S both decrease with depth, temperature must contribute the dominating density effect while salinity acts to destabilize the watercolumn – this leads to the double diffusive mode known as the *salt fingering* mode. On the other hand, if T and S both increase with depth the stratification is kept stable by the salinity contribution while the temperature term is unstable, and this leads to the *diffusive layering* mode of double diffusion. Except for the following short description of the salt fingering mode, we will restrict ourselves to studying only the diffusive layering mode in this thesis.

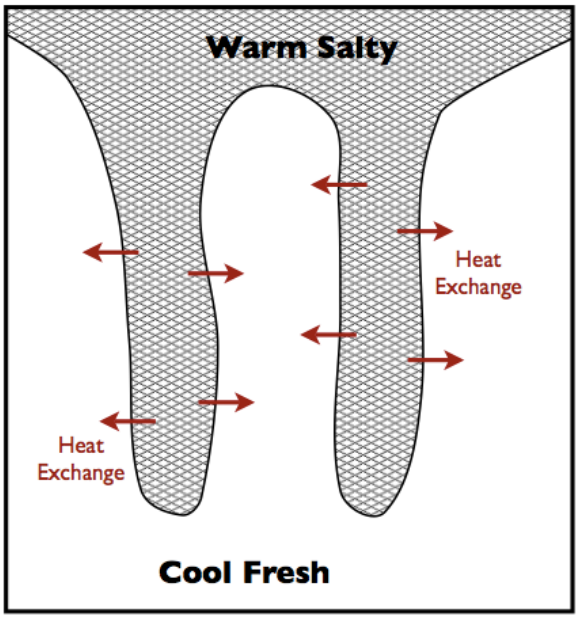

Figure 1.2 – A schematic of the salt fingering mode of double diffusion which occurs when warm salty water sits above relatively fresh, cold water. Long finger-like vertical intrusions which carry salt downwards, and across whose boundaries heat is exchanged by molecular diffusion, form spontaneously. Salt fingers occurs primarily in subtropical regions where evaporation creates relatively salty water near the surface.

1.2 The Salt Fingering Mode

In both modes of double diffusion, an instability causes convective motions that increase vertical transports relative to molecular diffusion. In the salt fingering case, the instability is easiest visualized by imagining a long metal conducting tube, open at both ends, extending down into a region of the ocean where temperature and salinity both decrease with depth. Initially, the water inside the tube is in thermal and static equilibrium with the surrounding water. However, if the water inside the tube is displaced upwards, it will be colder than the surrounding water and will quickly come to a new thermal equilibrium by thermal conduction through the metal pipe. The displaced water will also be less saline than the water directly outside the pipe, and since salt cannot diffuse through the metal, it will remain that way. The parcel is now at the same temperature but less salty than the surrounding water, is therefore lighter than the surrounding water, and will continue to rise. As it rises it will obtain more heat via conduction but will not become more salty – thus, the instability will grow and the parcel will continue rising. This phenomenon has come to be called the "perpetual salt fountain" since, once initiated, a tube transporting seawater through a watercolumn in this fashion will continue to do so until the vertical salt and temperature gradients have been equilibrated (Stommel, 1956).

In a natural system there is no conducting metal pipe to separate a water parcel from

its surrounding waters. However, the phenomenon can be reproduced *without* a physical boundary because the molecular diffusivity of heat in water is about one-hundred times higher than that of salt. Thus the difference in the speed at which heat and salt diffuse effectively takes the place of the conducting pipe, allowing a displaced water parcel to gain heat but not salt from its surroundings. Indeed, lab experiments (Stern, 1960) confirm that warm salty water above cold fresh water can spontaneously form elongated vertical intrusions, "salt fingers", which carry salt downwards and through which heat is exchanged by molecular diffusion (Figure 1.2).

The salt-fingering mode of double diffusion was the first to be reproduced in the lab and to be treated analytically (Stern, 1960). In the oceans, it is observed largely in subtropical regions where high evaporation tends to increase surface seawater salinity. For an example, see the results of the Carribean Sheets and Layers Transects (C-SALT) experiments (Schmitt et al., 1987). Historically, the salt-fingering mode has received more attention than the diffusive layering mode, though this may be more an artifact of convenience and habit rather than one of scientific motivation (Kelley et al., 2003). Though questions remain, a large body of research exists describing the salt fingering mode and its likely impact on oceanic mixing; for greater detail refer to Kunze (2003), Ruddick and Gargett (2003), and Schmitt (1994, 2003).

1.3 The Diffusive Layering Mode

The traditional way to conceptualize the instability of the diffusive layering mode is to imagine linear gradients with T and S both increasing with depth, in which a small parcel of water is displaced downwards. As in the salt fingering mode, heat diffuses into the parcel because the surrounding water is relatively warmer, while the salt content of the parcel remains virtually unchanged. The parcel is now lighter than its surrounding waters and begins to rise, overshooting its original position slightly because it has gained a density anomaly. After it has passed its initial height, it loses the heat it gained, plus a little more because its new surroundings are now cooler than they were initially, and again begins to sink – in this way, an oscillating instability initiates (Figure 1.3).

The linear stability analysis for concurrent one-dimensional linearly increasing T and S gradients bounded above and below is outlined comprehensively by Turner (1973). To give a brief review, the relevant non-dimensional parameters governing the problem are

$$R_\rho = \frac{\beta \Delta S}{\alpha \Delta T}\,, \qquad Ra = \frac{g\alpha \Delta T L^3}{\nu \kappa_T}\,, \qquad \text{and} \qquad Pr = \frac{\nu}{\kappa_T}\,. \tag{1.4}$$

The first parameter, R_ρ, is the density ratio and gives a measure of the stability of the

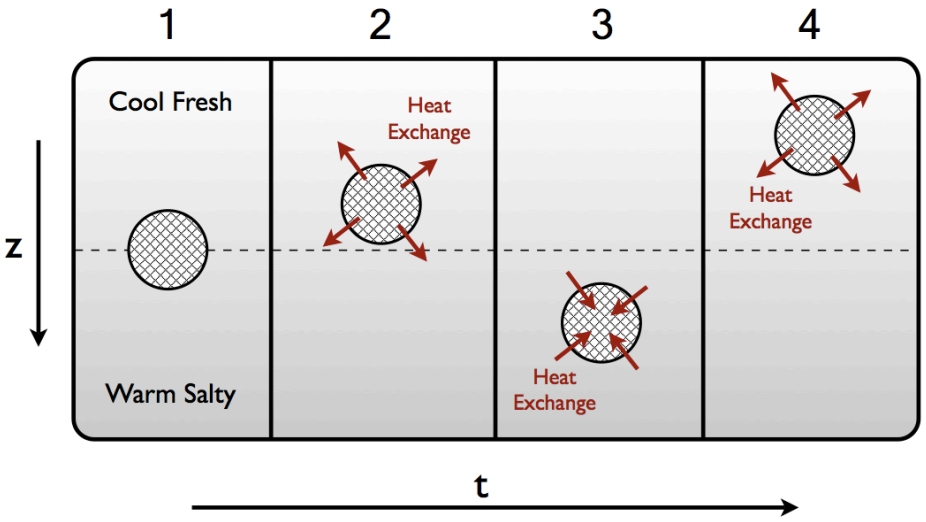

Figure 1.3 – The diffusive layering instability, based on T and S profiles that increase linearly with depth. Initially, the depicted water parcel is neutrally buoyant on the dashed line. As it is perturbed, the temperature of the parcel will equilibrate with its surroundings but the salt content of the parcel will not change much because of the relatively slower molecular diffusivity of salt. This initiates the growing oscillatory instability, as described in the text.

watercolumn; ΔS and ΔT are the differences in salinity and temperature between the top and bottom boundaries. The Rayleigh number Ra carries over directly from single-component, thermally driven convection; it is the ratio of the driving buoyancy forces to the retarding effects of viscosity and diffusivity. Here, g is the gravitational constant in m/s^2, ν the kinematic viscosity and κ_T the thermal diffusivity, both in m^2/s. L is the vertical length scale of the problem in meters. The last parameter Pr is the Prandtl number, the ratio of the kinematic viscosity to the thermal diffusivity, which in the ocean is $Pr \approx 6$.

From linear stability analysis, the double-diffusive instability is indeed oscillatory and is bounded by limits on the density ratio, with instability occurring only when

$$1 < R_\rho < \frac{Pr + 1}{Pr + \tau} \tag{1.5}$$

where τ is the ratio of the diffusivities of salt and heat. That is, $\tau = \kappa_S/\kappa_T \approx 0.01$ in seawater, suggesting that the instability initiates for $1 < R_\rho < 1.16$. However, there is reason to believe that in geophysical examples of double diffusive convection, the analysis of linear T and S profiles is not a useful way to describe the phenomenon.

In real geophysical situations, the definition of the density ratio has to be adapted in order to be relevant to the problem, and so it is standard to define a *background* density ratio

$$R_\rho^o = \frac{\beta(\partial S/\partial z)}{\alpha(\partial T/\partial z)} \tag{1.6}$$

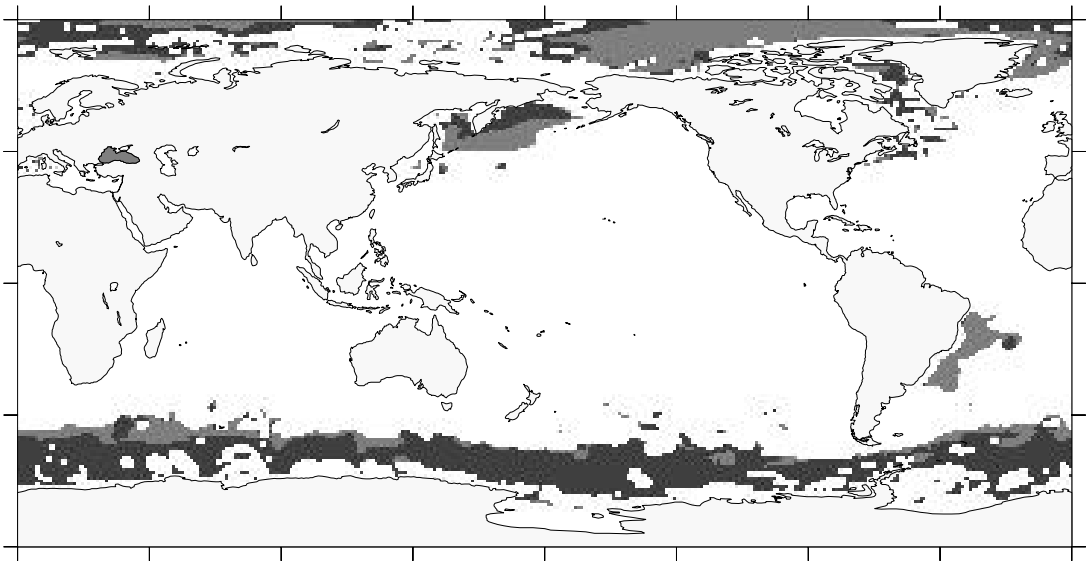

Figure 1.4 – Global susceptibility to diffusive layering – a map depicting regions where the large-scale stratification of the watercolumn is susceptible to double diffusion at some depth. Light shaded regions indicate areas where $3 < R_\rho^o < 10$ and dark shaded regions indicate areas with $1 < R_\rho^o < 3$. Note that this is a susceptibility map based strictly on gradients of T and S and not a map of observations of double diffusion. Reproduced from Kelley et al. (2003) with permission.

This definition incorporates the large-scale T and S gradients of the watercolumn, but is otherwise analogous to the single cell representation R_ρ. The background density ratio is the parameter used to determine the susceptibility to double diffusion of a given T and S stratification in the ocean. Strikingly, the diffusive layering mode is observed in oceans and lakes over the range $1 < R_\rho^o < 10$, and most observations tend to be in regions with $R_\rho^o > 2$, leading to the conclusion that the analysis of linear T and S profiles which gives the instability criterium Equation 1.5 is inappropriate for these real situations (Kelley et al., 2003; Padman and Dillon, 1987; Schmid et al., 2010, 2004; Timmermans et al., 2008).

Conditions favouring the diffusive layering mode are often found in high latitude regions and many of the most prominent examples come from measurements taken in the Arctic (Carmack et al., 2012; J. McDougall, 1983; Padman and Dillon, 1987, 1989; Polyakov et al., 2012; Timmermans et al., 2008). Double diffusive processes are also frequently observed in lakes with warm, subaquatic inflows, and in geothermally heated salt and pit lakes (Osborn, 1973; Schmid et al., 2004, 2010). Figure 1.4 highlights those regions of the world oceans where the stratification at some depth in the watercolumn is favourable to the diffusive layering mode of double diffusion.

The term *layering* in the name "double diffusive layering" refers to the characteristic thermohaline staircase structure that frequently accompanies this mode of double diffusion. Observations are usually characterized by a succession of thin layers with homogeneous T

and S properties that are separated from each other by even thinner, high-gradient interfaces (Figure 1.5). Observed layers tend to be on the order of one to ten meters high in oceanic settings, and interfaces are typically a few tens of centimetres high. Furthermore, Timmermans et al. (2008) have shown that, in the Arctic, individual layers can be traced horizontally for hundreds of kilometres, giving them an aspect ratio as high as 10^6.

In a simple conceptual model of the diffusive layering mode, convective motions maintain homogeneity within each layer, while molecular diffusion transports heat and salt through the interfaces that separate layers; hence, the term *diffusive* layering (Ruddick and Gargett, 2003). A schematic of this model is depicted in Figure 1.6. It is not clear from previous work how the step height, the interface height, or the temperature and salinity differences between layers are determined in a particular situation; a few parameterizations exist (Fedorov, 1988; Kelley, 1984), but these seem to give only rough agreement with observed staircase characteristics (Kelley et al., 2003; Schmid et al., 2004). Similarly, though a few recent papers have had some success modelling the initial stages and subsequent evolution of a double-diffusive thermohaline staircase (Noguchi and Niino, 2010a,b; Radko, 2003), the mechanism whereby layers form and are maintained is not evidently clear and has not been verified observationally.

1.4 The Diffusive Interface

In the context of a series of well-mixed layers separated by thin, high-gradient interfaces, we can resurrect R_ρ as a governing parameter if we adjust the meaning of ΔT and ΔS slightly. Here, these are the differences in the average T and S found in two successive mixed layers, and so R_ρ now quantifies the stability of the interface between those layers. Thus, in real geophysical situations, the two parameters R_ρ^o and R_ρ can both be used, but for different purposes: the first to assess the likelihood of double diffusion given a background stratification, the second to characterize the interface between observed double-diffusive layers.

The exact nature of the interface has been considered carefully, and it is of great interest to gain an understanding of its dynamics, since the interface is likely the seat of the double-diffusive instability which maintains homogeneity within the mixed layers. A recent approach to studying the interface is described by Carpenter et al. (2012), who model its stability by using a combination of linear stability analysis and direct numerical simulation. The primary difference to the analysis outlined in the previous section is that this study does not use linear profiles, but *erf* and *tanh* functions to more realistically model the shape of the interface.

The study by Carpenter et al. (2012) finds that the interface forms a gravitationally un-

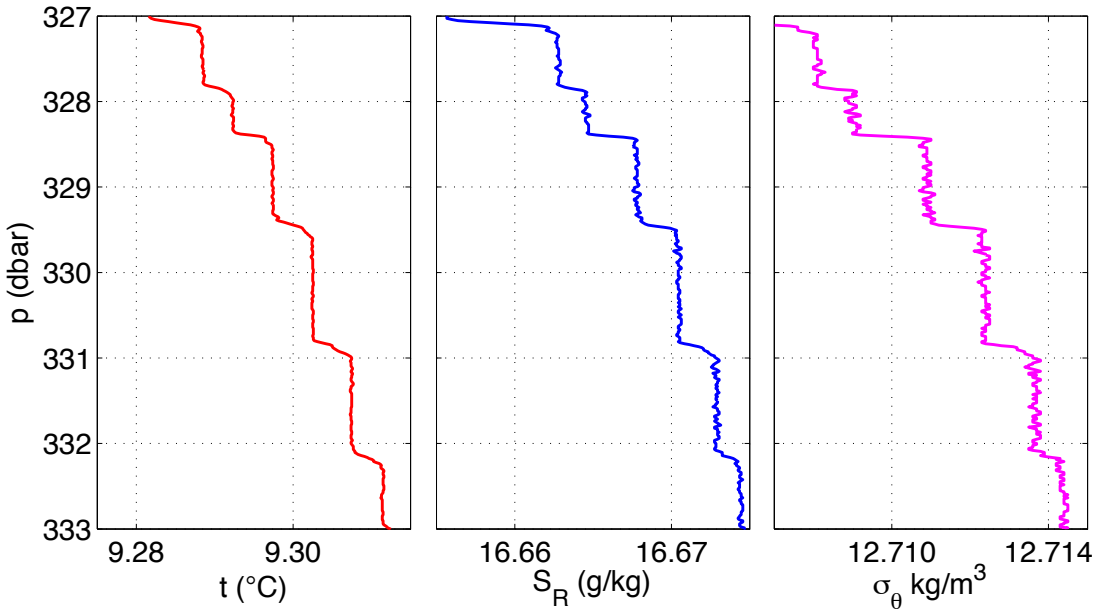

Figure 1.5 – An example of double diffusive layers, measured in Powell Lake. Shown are in-situ temperature t, Reference Salinity S_{R}, and potential density anomaly σ_θ. Small variations in S_{R} that are less than 0.0007 g/kg reflect the electronic noise of the conductivity probe, and these are propagated into the calculation of σ_θ. Temperature differences between layers are order 10^{-3} to 10^{-2} °C and salinity differences are order 10^{-3} to 10^{-2} g/kg. Well-mixed layers with a scale height of 1 to 10 m separated by thin high-gradient regions are characteristic of the diffusive layering mode of double diffusion. Profiles measured at station B03 (Figure 2.1).

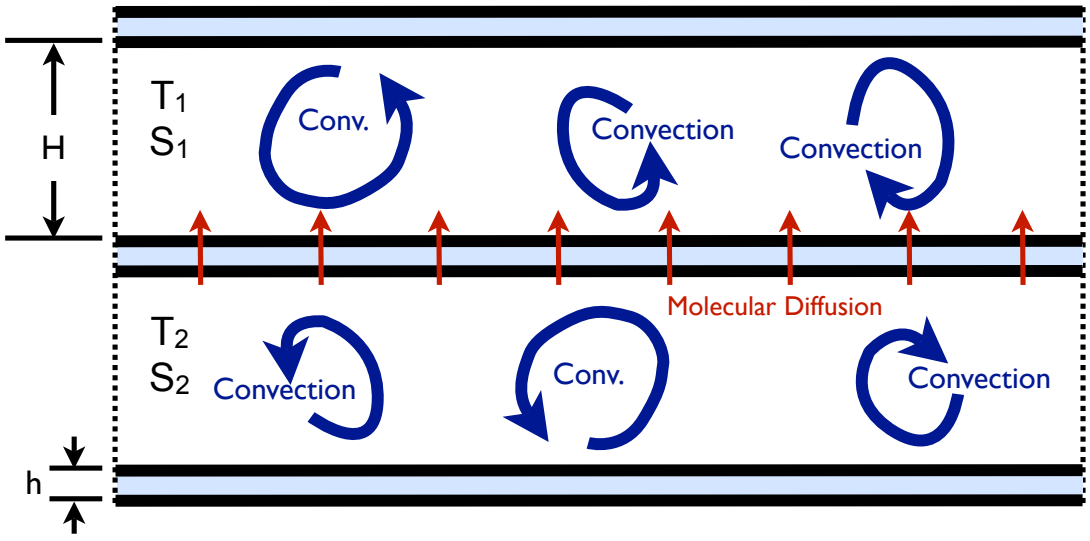

Figure 1.6 – A simplified schematic of two double diffusive layers and the interface between them. Convection homogenizes T and S within the layer while molecular diffusion is thought to carry heat and salt through the high-gradient interfaces. However, as discussed in the text, other transport mechanisms may also contribute. It is unknown what determines the cell height H, the interface height h, and the temperature and salinity differences between the two layers.

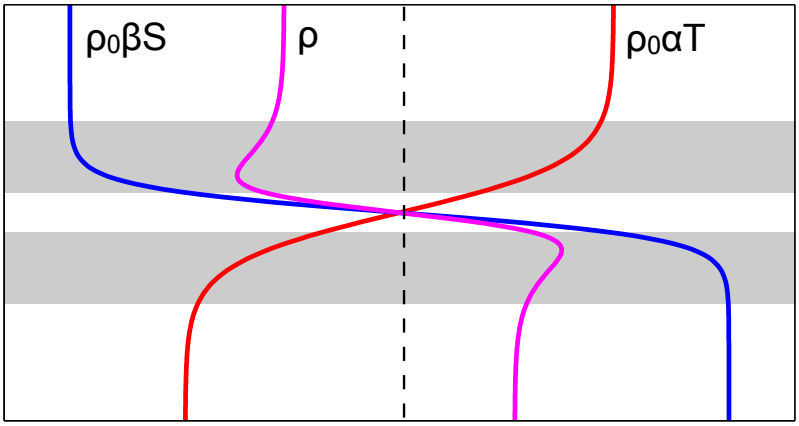

Figure 1.7 – Schematic of an interface between two double diffusive cells, depicting the unstable boundary layer model described by Linden and Shirtcliffe (1978) and Carpenter et al. (2012). Molecular diffusion thickens the temperature interface relative to the salinity interface, resulting in gravitationally unstable boundary layers at the edges of the interface (shaded in grey). These eventually break away as plumes which drive the convection in the double diffusive cells. T and S are normalized to density units.

stable boundary layer around a stable core. This occurs because heat diffuses through the interface faster than salt does, stretching the size of the T interface relative to that of the S interface (Figure 1.7). A convective instability initiates within the boundary layer, grows, and eventually forms a plume that breaks away from the core of the interface, adding to the convective mixing in the layer above it. Defining h_T and h_S as the heights of the temperature and salinity interfaces respectively and by scaling the one dimensional diffusion equation, we can expect the ratio $r_h = h_T/h_S$ to have an upper limit of $\sqrt{1/\tau} \approx 10$ if transport through the stable interface core is strictly by molecular diffusion.

Where the analysis of linear profiles resulted in the (observationally refuted) instability condition given by Equation 1.5, the analysis performed by Carpenter et al. (2012) allows for realistic values of the density ratio R_ρ. While not quoting a stability boundary, the authors report finding instability over the range $1 < R_\rho < 5$ which is in stark contrast to the stability boundary dictated by the analysis of linear profiles. This is good indication that the proposed interface model is a more realistic description of the double diffusive instability than the traditional study of linear profiles provided.

Despite these advances, there remains the open question whether transport through the interface is in fact limited by molecular diffusion, or whether a turbulent process is also active. While the former idea of a purely diffusive interface core is certainly the paradigm whereby double diffusive convection is typically envisioned (Figure 1.6), and while the simulations by Carpenter et al. (2012) support this model, there is also reason to question its completeness, and some past results (see below) would tend to support the notion that a secondary transport process may be active in the interface under certain conditions.

The interface model of a laminar, diffusive core surrounded on both sides by growing unstable boundary layers which eventually break away in plumes to support convection within the double diffusive cell was first proposed by Linden and Shirtcliffe (1978). However, even in this early work it was recognized that as R_ρ decreases and approaches unity, the convective motions within a cell may contribute to the vertical fluxes by entraining fluid across the interface. Marmorino and Caldwell (1976) perform lab experiments where they find that for high values of R_ρ the measured heat flux across the interface is that which would be expected by molecular conduction, but at low values of R_ρ the measured heat flux becomes larger than the conductive flux. The terms "high" and "low" are left somewhat ambiguous, but the experiments cover the approximate range $1.8 < R_\rho < 11$ and the authors quote that at $R_\rho = 2$ the net vertical heat flux is 2.5 times the conductive flux. Padman and Dillon (1987) also consider the possibility that heat fluxes through the interfaces they observed in the Arctic may be larger than is supported by molecular diffusion. Two studies of double diffusion in Lake Kivu by Schmid et al. (Schmid et al., 2004, 2010) do the same, mentioning that "there is some additional heat transport through the interfaces besides molecular diffusion due to intrusions of rising and sinking double-diffusive convective plumes".

1.5 Modelling Heat and Salt Fluxes

Once a double diffusive staircase is established it is desirable to quantify the net vertical fluxes of heat and salt through the layers. These are denoted F_H and F_S and have units $\mathrm{W/m^2}$ and $\mathrm{g/s/m^2}$ respectively. Observations show that double diffusive fluxes are significantly higher than would be supported by molecular diffusion alone through a similar background stratification (Kelley et al., 2003; Ruddick and Gargett, 2003). Measurements in Lake Kivu, in East Africa's Rift Valley, indicate they are enhanced relative to molecular fluxes by about an order of magnitude (Schmid et al., 2004, 2010) and the same is true of flux estimates in the Canada Basin of the Arctic Ocean (Padman and Dillon, 1987).

Parameterizations for estimating double diffusive fluxes were first developed by Turner (1965) and, though they have been refined, these have remained fundamentally unchanged to date. An overview is given below, with the recommendation to refer to Turner (1973) for greater detail. Double diffusive flux parameterizations are built in analogy to those of heat fluxes in single-component thermally driven convection where it assumed that, for sufficiently large Rayleigh number, the flux across a convecting cell is independent of the cell height H. The dimensionless heat flux, or Nusselt number, is given by

$$Nu = \frac{H F_H}{\rho \, c_p \, \kappa_T \Delta T} \tag{1.7}$$

and from dimensionality arguments, has the functional dependence

$$Nu = f(Ra, R_\rho, Pr, \tau) \tag{1.8}$$

where c_p is the specific heat in J/(kg °C) and H becomes the length scale in Ra.

By enforcing the assumption that fluxes are independent of H, choosing Ra as the governing parameter and ignoring any dependence on Pr and τ (which are nearly constant), it is possible to refine the form of Equation 1.8 to yield

$$Nu = f_1(R_\rho)\, Ra^{1/3} \tag{1.9}$$

where $f_1(R_\rho)$ is an unknown function of the density ratio to be determined experimentally. By substituting the definitions of Nu and Ra, we can retrieve the dimensional equivalent of Equation 1.9:

$$F_H = f_1(R_\rho)\, \rho\, c_p \left(\frac{\alpha g \kappa_T}{Pr}\right)^{1/3} (\Delta T)^{4/3} \tag{1.10}$$

This expression and similar ones have come to be known as "4/3 Flux Laws" because of the heat flux dependence on $(\Delta T)^{4/3}$. However, for the purposes of this study we will refer to Equation 1.10 more simply as a flux parameterization rather than a *law*.

A similar argument to that outlined above leads to an expression for the dimensionless salt flux

$$\frac{H F_S}{\rho \kappa_S \Delta S} = f_2(R_\rho)\, Ra^{1/3} \tag{1.11}$$

where f_2 is again an unknown function of the density ratio. The Rayleigh number is chosen as a governing parameter for the salt flux, in analogy to the heat flux, because the convection that carries salt across the cell is thermally driven.

From Equations 1.9 and 1.11 it is possible to construct a dimensionless flux ratio

$$R_F \equiv \frac{c_p\, \beta F_S}{\alpha F_H} = \tau\, f_4(R_\rho) \tag{1.12}$$

which, if the preceding arguments are correct, depends only on the density ratio and the physical properties of seawater. However, regardless of the correctness of the arguments leading to the right hand side of Equation 1.12, the ratio of salt to heat fluxes is a quantity that can be measured in a lab experiment. This experiment was carried out by Turner (1965) as well as a few other researchers (Crapper, 1975; Newell, 1984), and these sources agree that R_F decreases sharply from 1 at low R_ρ and is near constant at

$$R_F \approx 0.15 \tag{1.13}$$

over the range $2 < R_\rho < 8$. This result is often used in observational studies as it is usually

difficult to obtain independent estimates of F_H and F_S in geophysical situations.

A considerable amount of work by different authors (Crapper, 1975; Kelley, 1990; Marmorino and Caldwell, 1976; Turner, 1965) has also gone into determining the factor f_1 of Equation 1.10. We will use the formulation developed by Kelley (1990) because it has been used in a number of recent studies (Carmack et al., 2012; Polyakov et al., 2012; Schmid et al., 2010; Timmermans et al., 2008) and has met with reasonably good success at estimating double diffusive fluxes. Kelley creates an empirical fit to a collection of previous lab-based results, resulting in a factor for Equation 1.10 with the form

$$f_1(R_\rho) = 0.0032 \exp\left(4.8/R_\rho^{0.72}\right) \tag{1.14}$$

Equations 1.10 and 1.14 together form what we will refer to as the Kelley 4/3 flux parameterization:

$$F_K = 0.0032 \exp(4.8/R_\rho^{0.72})\, \rho\, c_p \left(\frac{\alpha g \kappa_T}{Pr}\right)^{1/3} (\Delta T)^{4/3} \tag{1.15}$$

In conjunction with the laboratory derived flux ratio (1.13), this allows for estimates of double diffusive fluxes through a thermohaline staircase based strictly on observations of T. However, the accuracy of the flux parameterizations has been called into question as a number of unresolved inconsistencies remain.

Firstly, there is theoretical and experimental evidence suggesting that the classical fluid dynamics result for single-component thermally driven (Rayleigh-Bénard) convection

$$Nu \propto Ra^{1/3} \tag{1.16}$$

may be incorrect or only applicable over certain parameter ranges (Castaing et al., 1989; Kelley, 1990). Indeed, there is a large body of work describing Rayleigh-Bénard convection, and it is a much more complex field of study than this simple scaling argument suggests. For further reading, see Grossmann and Lohse (2001) and Heslot et al. (1987).

The uncertain grounding of Equation 1.16 also casts doubts on the correctness of its derivative Equation 1.9. If the model for the single-component convection parameterization is incorrect or incomplete, we would expect the more complicated double diffusive parameterization to be likewise. A simple one-cell analytical model developed by Kelley (1990) suggests that the exponent in Equation 1.9 may be variable and near the range 0.27 ± 0.02. If this is the case, then the traditional 4/3 parameterizations would overestimate fluxes by up to about 30% in oceanographic settings. However, because of a lack of more conclusive evidence, both exponents 1/3 and 0.27 ± 0.02 continue to be used to estimate heat fluxes. Current work by Sommer and Wüest (2013) suggests that an exponent that varies with Ra could produce more consistent results.

The applicability of double diffusive flux parameterizations remains uncertain in part because of a lack of observational evidence verifying their accuracy. While observations of double diffusive layers are not rare, it is difficult to obtain independent, well-resolved estimates of vertical heat fluxes by which to calibrate the parameterizations. One common approach is to assume pure molecular diffusion through the interfaces and use microstructure measurements to calculate the diffusive flux:

$$F_H = \rho c_p \kappa_T (\partial T / \partial z) \tag{1.17}$$

The heat flux calculated using this method should be viewed as a lower limit since it is only accurate if the interface core is strictly laminar. Padman and Dillon (1987) found the two methods to agree within about a factor of 4 in the Beaufort Sea; Schmid et al. (2010) observed agreement within a factor of 2 from measurements in Lake Kivu; and Timmermans et al. (2008) also cite agreement within approximately a factor of 2 in the Canada Basin of the Arctic.

The present study of double diffusion in Powell Lake is unique because it is possible to develop and verify an independent measure of the vertical heat flux through the thermohaline staircase (see Section 1.6 below). As will be shown, this extra condition gives new insight into the nature of the interface and allows us to make comparisons to the 4/3 flux parameterizations with much greater precision than has been done before. If the 4/3 exponent is indeed incorrect, it would suggest that the underlying assumption that fluxes are independent of H is invalid in the context of double diffusion. We present results in this study that indicate that this may indeed be the case and that it may be possible to develop a new parameterization which more accurately encapsulates the physics of double diffusion.

1.6 Powell Lake

Powell Lake is a glacially formed ex-fjord on the south-west coast of British Columbia, Canada (Figure 1.8). Situated 150 km north of Vancouver near the city of Powell River, the lake is 40 km long, 2-4 km wide, and has a maximum depth of 350 m. It displays the characteristics typical of glacial fjords including steep sides and sills separating largely flat-bottomed basins. Following a bathymetry study by Mathews (1962), the lake can be divided into six basins: the East and South Basins are permanently stratified and contain relatively warmer relic seawater at depth with maximum salinities of 4.5 and 16.5 g/kg respectively; the West Basin and the three northern most basins are holomictic and have almost no measurable salt content (Figure 1.9). The presence of seawater in the lake was originally discovered by Williams et al. (1961) who also noted that the deep waters are anoxic and contain high sulphide and methane contents while having a “distinct yellow

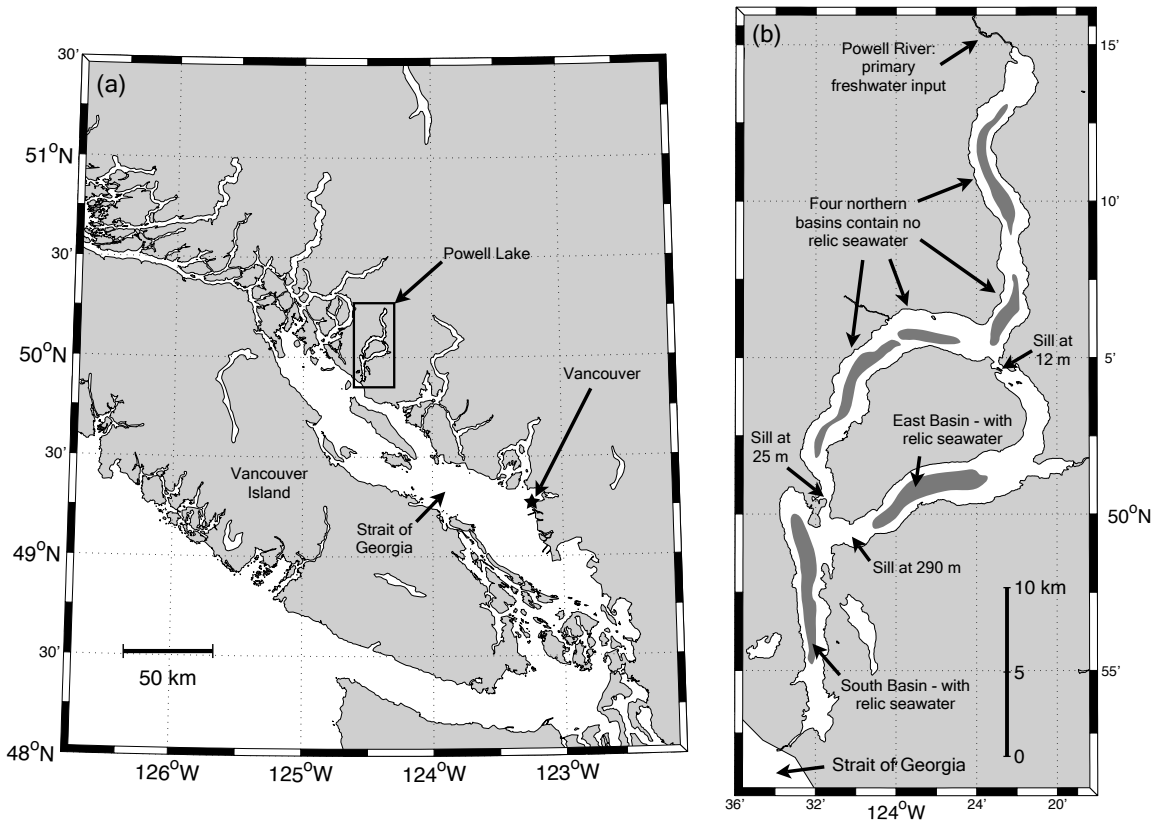

Figure 1.8 – Maps depicting (a) south-western British Columbia and (b) Powell Lake, a glacially formed ex-fjord adjacent to the Strait of Georgia. The lake was separated from the Strait by the emergence of a sill about 10,000-13,000 years ago. The six flat-bottomed basins of Powell Lake are shaded in dark grey, following the bathymetry study of Mathews (1962). The South and East Basins are permanently stratified and contain relic seawater and are separated from the rest of the lake by shallow sills.

colour which... was evidently due to dissolved organic matter". The supersaturated gas concentrations, as evidenced by degassing at atmospheric pressure, and distinct colouring are also present in the lake today.

Freshwater input to Powell Lake by river run-off is substantial and is largely at the northern head of the lake. Net flow rates through the dam at the south end of the lake average about 3×10^9 m^3/yr (Sanderson et al., 1986). However, because the sills separating the individual basins are quite shallow, any turbidity currents are likely isolated to the northern end of the lake. Flushing by turbidity currents is a likely explanation for the absence of salt water in the northern basins. At the southern end, the lake is separated from the adjacent Strait of Georgia by a rocky sill on which a hydro-electric dam was built in the early 20th century to supply electricity to the local pulp-and-paper mill, stabilizing the current water level of the lake to be about 50 m above sea level. Below approximately 130 m depth, the waters in the South Basin are completely anoxic indicating that there is no seasonal signal and little turbulent mixing below this depth.

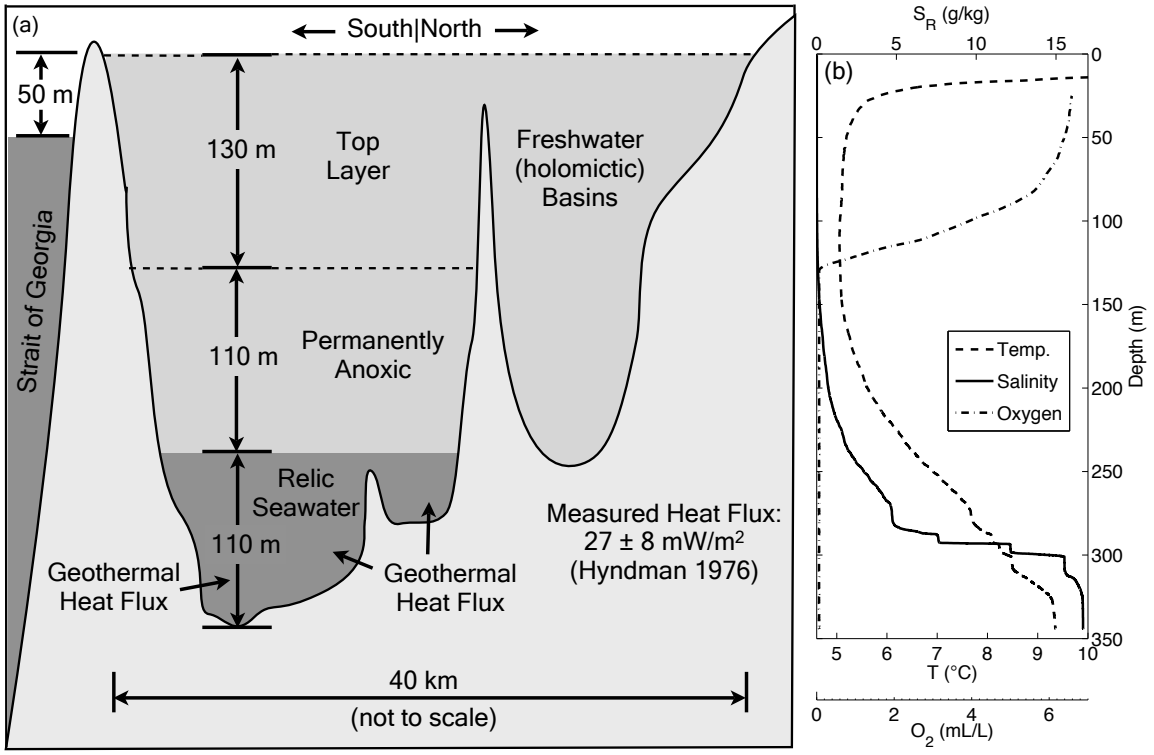

Figure 1.9 – (a) Schematic cross-section of Powell Lake, not drawn to scale laterally. Anoxia is permanent below 110 m depth indicating limited vertical mixing. Relic seawater is found below 240 m depth and is geothermally warmed by a heat flux of 27 ± 8 mW/m^2. (b) Temperature, Reference Salinity, and dissolved oxygen profiles in the middle of the south basin, the deepest part of Powell Lake.

Geological considerations suggest that Powell Lake was isolated from the adjacent Strait of Georgia $10,000$ – $13,000$ years ago by isostatic rebound (Mathews et al., 1970). Sanderson et al. (1986) model the subsequent evolution of the lake and are able to successfully reproduce the general temperature and salinity structure in the South Basin by considering molecular diffusion as the dominant process transporting heat and salt from the deep waters to the fresh upper layer; from here, salts are subsequently flushed from the lake. Descending through the watercolumn, temperature decreases quickly with depth to near 5 °C at 125 m (representing the depth of winter mixing) and then begins to increase quasi-linearly to a maximum of 9.5 °C at the bottom (Figure 1.9). Salinity is almost zero at the surface and also begins to increase at about 125 m; there is a very strong halocline between 270 and 320 m depth and the maximum salinity occurs at the bottom of the watercolumn. Double diffusive layers (Figure 1.5) are observed in the lower gradient regions between 301 – 310 m and 325 – 350 m and are most clearly defined in the latter.

Temperature increases with depth because there is a geothermal heat flux into the bottom of the lake. Hyndman (1976) measured this flux to be 27 ± 8 mW/m^2 from sediment core samples. This is a number similar to those measured in other nearby inlets of southwestern

British Columbia. Since there are no other sources of heat, the relative linearity of the temperature profile below the anoxic boundary, especially between 310 and 325 m depth, supports the notion that molecular diffusion is the dominant vertical transport mechanism in these sections of the watercolumn. This can be validified by corroborating the strength of the observed linear temperature gradient to the measured heat flux (Section 4.3).

To our knowledge there are six previous academic studies directly related to Powell Lake. The first is the study by Williams et al. mentioned above which outlines the discovery of the salt layer at the bottom of the lake (Williams et al., 1961). This was followed soon after by the bathymetry study by Mathews (1962) and later by the first (and until now, only) temperature microstructure study in Powell Lake by Osborn (1973). This later study correctly hypothesizes that the double diffusive instability may be active in the deepest parts of the lake and presents measurements which show "characteristic doubly diffusive layers in the region between 3–5 m above the bottom". Interestingly, Osborn points out that there may be a relationship between the strength of the heat flux and the height of double diffusive layers. This publication was followed by the Hyndman (1976) study of heat flux measurements in two lakes, including Powell Lake, and a number of nearby inlets, and the vertical diffusion study by Sanderson et al. attempting to model the evolution of the large-scale temperature and salinity profiles (Sanderson et al., 1986). Finally, the most recent study was a chemical study of sulphur speciation and pyrite formation in meromictic Powell and Sakinaw Lakes (Perry and Pedersen, 1993).

1.7 Motivation

Double diffusion is a global phenomenon that may have the potential to impact ocean circulation on large spatial scales (Ruddick and Gargett, 2003). As an example, double diffusive signatures are observed over large portions of the Arctic ocean and are especially prominent in the thermocline between the cool, fresh surface waters and the relatively warmer and saltier Atlantic Water layer that lies between 250 and 800 m depth. The heat content in this warmer, deeper layer is enough to melt all the Arctic sea ice if it were transported to the surface (Rudels et al., 2004). Since double diffusive fluxes appear to be the dominant transport mechanism across the central Canada basin thermocline (Timmermans et al., 2008), understanding and quantifying these is of primary importance to forecasting environmental changes in the Arctic.

Some East African rift and crater lakes also exhibit double diffusive signatures, and gaining an understanding of these is also critical because a number of African lakes naturally accumulate dangerously high concentrations of methane and carbon dioxide gases. When gas concentrations in the deep waters of these lakes reach supersaturation, a disturbance

in the watercolumn can result in a large uncontrolled gas eruption at the surface. This can have catastrophic consequences when the released gasses displace the breathable air in the surrounding communities; in recent history, more than 1700 people died when Cameroonian crater lakes Monoun and Nyos erupted large quantities of carbon dioxide gas in the 1980s (Sigurdsson et al., 1987; Sigvaldason, 1989). In Lake Nyos, double diffusive steps are observed in the thermocline that separates the gas-enriched deep waters from the surface, and while it is more probable that the gas eruption was triggered by a localized landslide, double diffusion has been proposed as a possible mechanism responsible for initiating the eruption (Schmid et al., 2004). Since the net effect of double diffusion is to equilibrate density gradients, it is conceivable that double diffusive effects homogenized sections of the watercolumn, thus allowing an overturning event to release the gases which had until then been trapped at depth.

Lastly, it is worthwhile mentioning that double diffusive phenomena are studied in fields outside of oceanography. Most pointedly perhaps, double diffusion is a current research topic in astrophysics (Bruenn and Dineva, 1996; Rosenblum et al., 2011) and researchers may even straddle fields, applying their knowledge to both the oceanography and the astrophysics context (Merryfield, 1995, 2000). Indeed, since the phenomenon is the same, much of the formalism and the language are consistent between the two fields, and there is explicit overlap between their research approaches (e.g. compare Rosenblum et al. (2011)). Applications of double diffusion are also found in chemistry, geology, geophysics, metallurgy, and engineering; an outline of how double diffusion relates to each of these fields can be found in the proceedings of a cross-disciplinary engineering conference dedicated to double diffusive convection (Chen and Johnson, 1984).

Powell Lake presents a unique opportunity to study double diffusive convection because the presence of warm relic seawater capped by an anoxic boundary at 130 m depth, the linearity of the temperature gradient, the lack of tidal and geostrophic effects, and the absence of turbidity currents all suggest that the deep waters of Powell Lake are extremely quiescent. The large majority of the double diffusive layers we observe appear undisturbed and so free from the influence of external mixing processes. In this regard, the deep waters of Powell Lake are a natural laboratory, and the degree to which the double diffusive process is isolated from other transport mechanism is, to our knowledge, unmatched in any other natural system that has been studied.

Because double diffusion is naturally decoupled from other processes in Powell Lake, it is possible to collect many measurements of extremely well-resolved double diffusive layers over large scales in time and space. This allows us to examine details regarding the nature of the diffusive interface and associated instability which have previously been only modelled. This will help to verify or modify the existing model of a diffusive interface core through which transport is limited by molecular diffusion.

Furthermore, again owing to the relative quiescence of Powell Lake, we are able to gain multiple separately derived estimates for the heat flux through double diffusive layers to which we can compare existing flux parameterizations. This allows us to verify the predictive ability of the 4/3 flux parameterizations and see their limitations with a precision that we have not seen presented before in a geophysical study. We hope that this will enable further conversation with the aim of refining parameterizations and addressing some of their current inconsistencies.

1.8 Objective

In light of the motivating features discussed above, the objective of this study is to delineate the state of double diffusion in the deep basin of Powell Lake in order to provide new insights into the nature of double diffusive layers, the interfaces separating layers, and the fluxes of heat and salt transported vertically through the layers. A unique characteristic of this study is that the vertical heat flux through the double diffusive staircase can be estimated by independent measures. This allows us to test the scaling that underlies current double diffusive flux parameterizations. Furthermore, an independent estimate of the vertical heat flux provides a comparison by which to confirm whether transport through the interface between mixed layers is indeed controlled by molecular diffusion.

In order to accomplish our objective, we carefully measure closely spaced fine-scale temperature and salinity structures within the staircase and over the length of the basin. Using a simple but robust algorithm, we detect individual layer/interface boundaries in both temperature and salinity from measured profiles, and thereby compile an extensive dataset of staircase properties on which to build our conclusions.

Chapter 2

Research Methods

2.1 Measurements and Equipment

The data presented here consists of 39 high vertical resolution conductivity-temperature-depth (CTD) measurement casts using a Seabird SBE-25 outfitted with a SBE-3F temperature sensor and a SBE-4 conductivity sensor. CTD casts were taken at 21 distinct stations along the length of the South Basin, encompassing nearly a full lateral transect of the flat bottomed portion where double-diffusive layers are observed (Figure 2.1). The 21 stations are spaced 200–300 m apart. All stations were measured at least once; stations B01–B06 and B08–B12 were measured twice, and station B07 was measured eight times. Measurements are from July 2012 and were made over a span of two days. Of the 39 CTD casts, seven extend from the surface to the lake bottom; the rest begin at 250 m depth and extend to the bottom. The instrument was equipped with a landing-device, allowing us to consistently measure up to within 55 cm of the lake sediments. In addition to the high resolution measurements along the length of the lake, we obtained six lower resolution CTD casts in a line across the South Basin on an earlier trip in June 2012.

The SBE-25 sampled at its maximum frequency of 8 Hz. We lowered the instrument through the double diffusive portion of the watercolumn at an extremely low average speed of 11 cm/s, yielding a mean vertical measurement resolution of 1.4 cm. Compare this to standard CTD sampling procedures which typically measure at 4 Hz and a speed of 100 cm/s, giving a vertical resolution of 25 cm.

The resolution of the temperature sensor is 0.0001 °C and the electronic noise in the temperature measurement tends to be less than 0.0005 °C. The electronic noise in the conductivity cell likewise tends to be less than 0.0005 mS/cm. This results in a salinity signal with a resolution of 0.0001 g/kg and an observed electronic noise level of 0.0007 g/kg. The quoted electronic noise levels are representative of the in-situ fluctuations of the temperature and

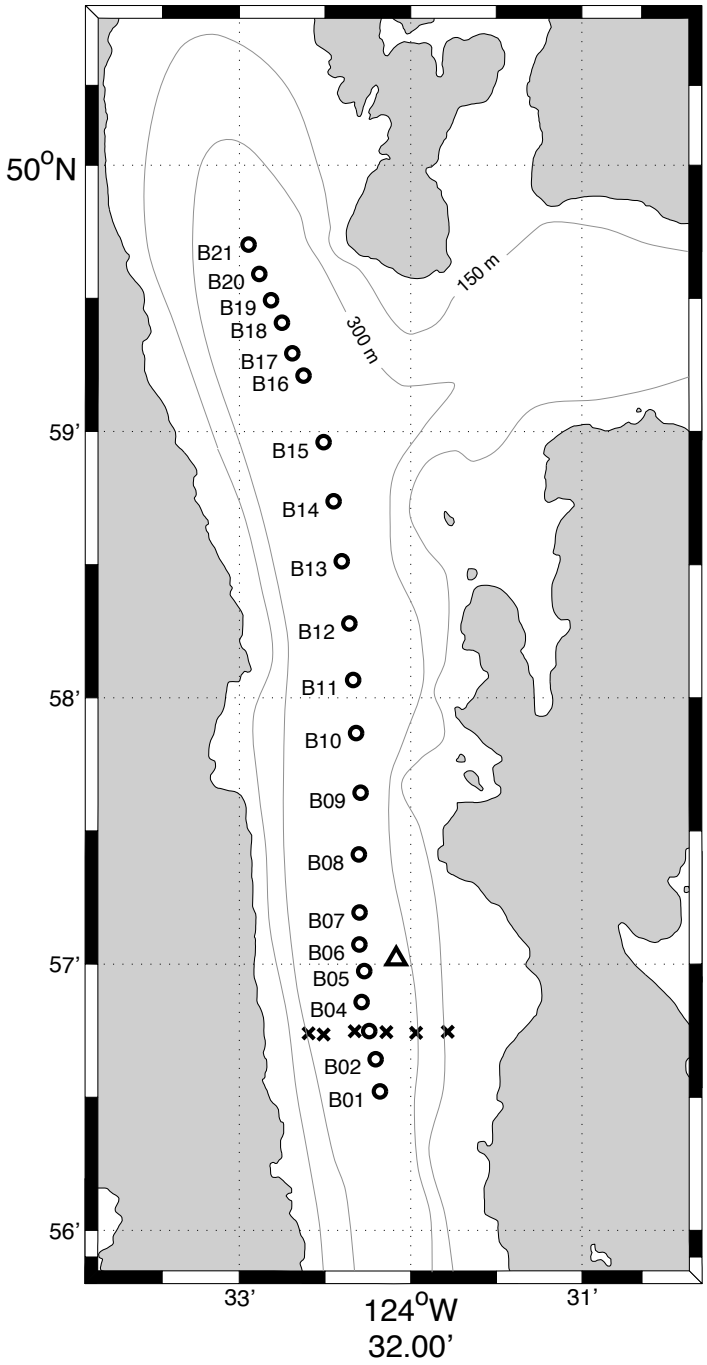

Figure 2.1 – Measurement locations in the South Basin, depicting the 21 stations at which we measure the double-diffusive staircase (open circles), as well as the locations of six lower resolution cross-lake CTD casts (x-marks). Depth contours follow Mathews (1962) and are drawn at 150 m and 300 m. The triangle marks the location of an in-situ temperature mooring in the double-diffusive staircase.

conductivity sensors.

The quality of our measurements may also be limited by the response time of the temperature and conductivity sensors. The temperature sensor has a known response time of 0.1 s; therefore, at a lowering rate of 11 cm/s, an instantaneous temperature change would be recorded as a gradual increase in temperature over 1.1 cm.

The response time of the conductivity cell is slightly more complicated to calculate. From the sensor specifications, the required time to reach 68% of the final conductivity value after a step change in salinity is 0.06 s. In practice, the response time is limited by the amount of time required to flush the conductivity cell because the actual conductivity measurement is an average over the finite volume of the cell. The conductivity cell has a volume of 2.4 mL, and the measured flow rate of the instrument's pump which fills the cell is 15 mL/s. Consequently, it takes 0.16 s to flush the interior volume of the conductivity cell. In this time, at a fall rate of 11 cm/s, the instrument covers a vertical distance of 1.8 cm. That is, an instantaneous salinity change would be recorded as a gradual increase in conductivity over 1.8 cm.

In practice, the finite sensor response times have the effect of smoothing sharp changes in temperature and conductivity measurements over scales of one or two centimetres. We do not correct for the smoothing effect as its length scale is still substantially smaller than the observed interface height which tends to be between 10 and 20 cm in both temperature and salinity (Section 3.1). Furthermore, the smoothing effect occurs over approximately the same distance as the mean vertical measurement resolution of 1.5 cm, meaning it is largely unnoticeable in our measurements.

We additionally find that the quality of our measurements depends on the stability of the lowering rate of the instrument; the stability of the lowering rate in turn depends on the surface motions of the lake because, unlike a true microstructure profiler, the CTD is coupled to the boat by a physical wire. This means that boat motion due to surface wind waves (or other causes) translates to vertical motions of the instrument which artifically introduce localized fluctuations and thereby increase the uncertainty in our measurements. Consequently, we took great care to measure only when conditions on the lake are ideal and the boat experiences minimal motion. Ideal conditions include low wind speeds (estimated less than 5 km/h) and no noticeable wind waves; because we found that these conditions typically occur between sunset and sunrise, we performed our CTD casts at night.

Lastly, the conductivity measurement of a parcel of water occurs approximately 0.2 s after the corresponding temperature measurement. This is easily corrected by aligning the conductivity measurement with the temperature measurement with a fixed time delay of 0.2 s.

2.2 Layer Evaluation

Unless mentioned otherwise, we quote in-situ temperature t and Reference Salinity S_R for all results. We choose to use in-situ temperature in place of conservative temperature because this is the correct temperature variable to use when discussing molecular diffusion. Formally, heat diffuses along gradients of *in-situ* temperature rather than gradients of conservative temperature (which is designed to conserve heat content under mixing), though in our measurements the difference is largely negligible. Since the chemical composition of the relic seawater in Powell Lake is similar to that of present-day seawater, we use the measured conductivity and temperature to compute Reference Salinity according to TEOS-10 (IOC et al., 2010), assuming a salinity anomaly of zero. When plotting depth profiles, we use in-situ pressure p in dbar as a proxy for depth.

In order to automate the detection of double diffusive layer and interface boundaries, we implement an algorithm similar to that described by Polyakov et al. (2012). For the purpose of illustration, consider first a temperature profile (Figure 2.2a). From the measured t staircase, we extract the mean background signal by applying a 0.75 m low-pass running mean filter. The difference δt between the actual and background signals oscillates around zero with sharply defined peaks at the edges between layers and interfaces. Therefore, by identifying the peaks in δt, we can identify the locations of the mixed layers and their corresponding interfaces. We apply the same algorithm separately to the salinity profiles (Figure 2.2b) to derive independent layer and interface properties in t and S_R. Individual layers are more easily identified in t than in S_R because the electronic noise level of the instrument relative to the signal difference between successive layers is higher for conductivity than it is for temperature; nevertheless, our measurements are precise enough that we are able to identify the layer and interface boundaries with confidence in S_R as well as in t. In fact, we mark mixed layers only if they are clearly identifiable in both t and S_R, and if they have a minimum height of 7 cm.

We define Δt and ΔS_R as the differences in the average in-situ temperature and Reference Salinity between consecutive layers (Figure 2.3). The interface heights in t and S_R as calculated by the layer-finding algorithm are given by h_t and h_S respectively, and the mixed layer height is labelled H. We use the temperature profiles to determine the layer height, and we do not differentiate between the layer heights in the temperature and salinity profiles because the difference between the two relative to their average is small. This is not the case for the heights of the interfaces, where we expect diffusion to thicken the temperature interface more quickly than the salinity interface, motivating us to characterize the two interfaces separately.

Despite the high quality of our measurements, it is still necessary to apply some high-frequency filtering in order to successfully apply the layer-finding algorithm to our data.

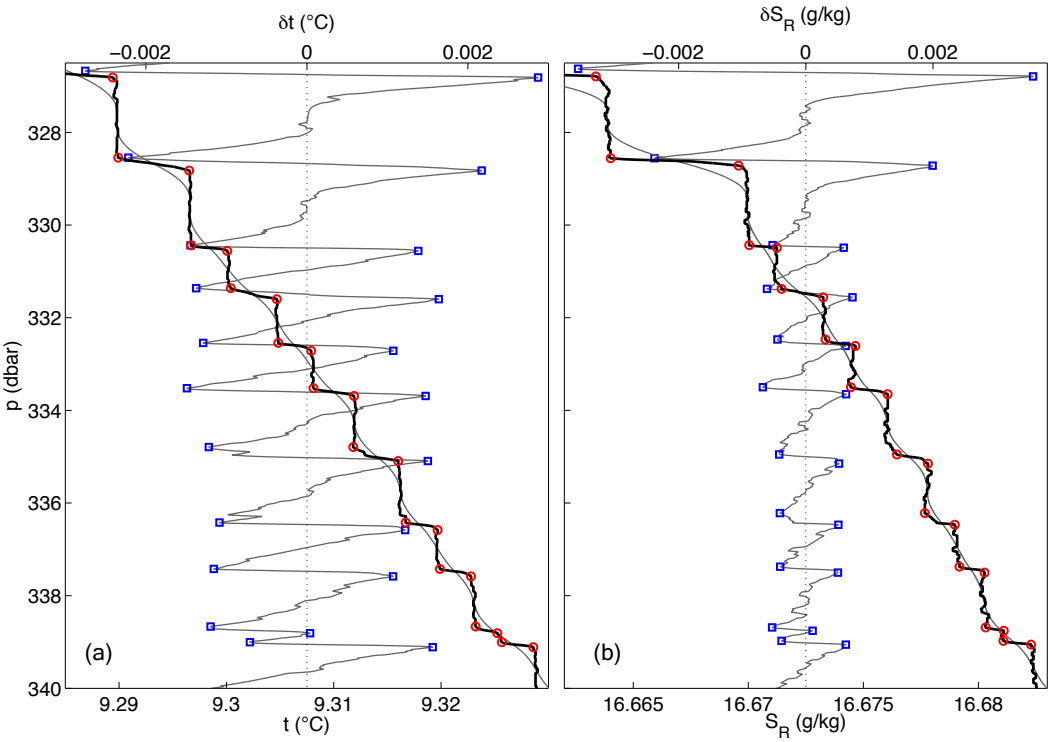

Figure 2.2 – Our mixed layer and interface detection algorithm, similar to that described by Polyakov et al. (2012). The measured profile (t left and S_R right) is shown by the thick black line. The mean background signal (smooth grey line behind the profile) is derived using a 0.75 m low-pass filter, and the difference (δt and δS_R for temperature and salinity respectively) between the measured and background profiles is shown by the alternately peaking and troughing grey line. Peaks and troughs in δt and δS_R, marked by open squares, correspond to the edges of diffusive interfaces which are marked by open circles on the profiles. Peaks and troughs are most clearly seen in δt but are still unmistakeably evident in δS_R. Mixed layers are marked if their height is at least 7 cm. Example profiles shown here are taken at station B18.

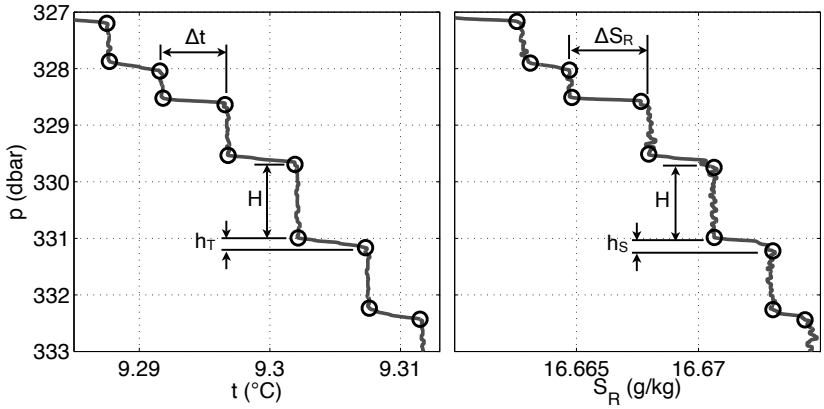

Figure 2.3 – Example close-up of a few layers in t (left) and S_R (right), measured at station B04. The definitions for the temperature and salinity differences between layers, Δt and ΔS_R respectively, are shown along with those for the mixed layer height H, and the temperature and salinity interface heights, h_T and h_S. The layer-interface boundaries as determined by the layer-finding algorithm are depicted by open circles.

To accomplish this, we use a 12.5 cm running median filter (Barner and Arce, 1998) which preserves the sharp interface/layer boundaries while successfully removing some of the electronic noise in the temperature and conductivity signals.

The only independent variable in calculating the difference profiles δt and δS_{R} is the size of the low-pass filter used to derive the background signals. We choose the window size 0.75 m because this is typical of the observed layer height. In order to test the robustness of our layer-finding algorithm, we choose a representative profile and perform the calculation using a 0.50 m and 1.00 m window. We find that on average H changes by less than 2% for the 0.50 m window and less than 1% for the 1.00 m window, h_T changes by less than 8% and 2% respectively, and h_S changes by less than 12% and 2% respectively. These changes are small enough to neglect in much of the following analysis, but we must consider them when interpreting any observed differences between the temperature and salinity interfaces, as will be discussed below. Note that the changes in h_T and h_S are correlated with each other and anti-correlated with those in H.

Chapter 3

Results

3.1 CTD Measurements

In the South Basin of Powell Lake, temperature and salinity both increase monotonically with depth from 250 m to the lake bottom at 348 m (Figure 3.1). Temperature increases consistently and quasi-linearly while salinity increases most rapidly from 280–300 m. Both profiles have high-gradient regions between 250–270 m, 282–287 m, 293–294 m, 298–301 m, and 309–324 m. The intermediate depths between these regions and below the last one exhibit much lower gradients in t and S_{R}, forming a large-scale step-like structure with a scale height of a few meters. This should not be confused with the double-diffusive layers we report on in this study, which are found within the larger steps described here; it is unclear how the large-scale steps developed.

There are three regions over which double-diffusive layers are observed. All three regions have background density ratios that reach below 2; however, double-diffusive layering is most clearly defined and most consistent in the deepest region, between 324 m and the bottom of the watercolumn (Figure 3.2). Here, the density ratio ranges approximately over $2 \leq R_\rho^o < 6$, with the lowest values observed near the middle of the staircase. In the shallowest region, between 294–297 m, the layers are observed only near the northern end of the basin; in the second region between 301–309 m, they are observed over most of the length of the basin, but the double diffusive layer/interface boundaries are not as clear as they are in the deepest region. For this reason, unless mentioned otherwise, the following analysis is restricted to the lower staircase only, which extends to within 1 metre of the bottom of the lake. It is also worth noting that the density ratio between 310 – 323 m depth, where there are no double-diffusive signatures, varies between $4 \leq R_\rho^o < 12$ so that there is some overlap in the respective ranges of R_ρ^o where double diffusive steps are and are not observed.

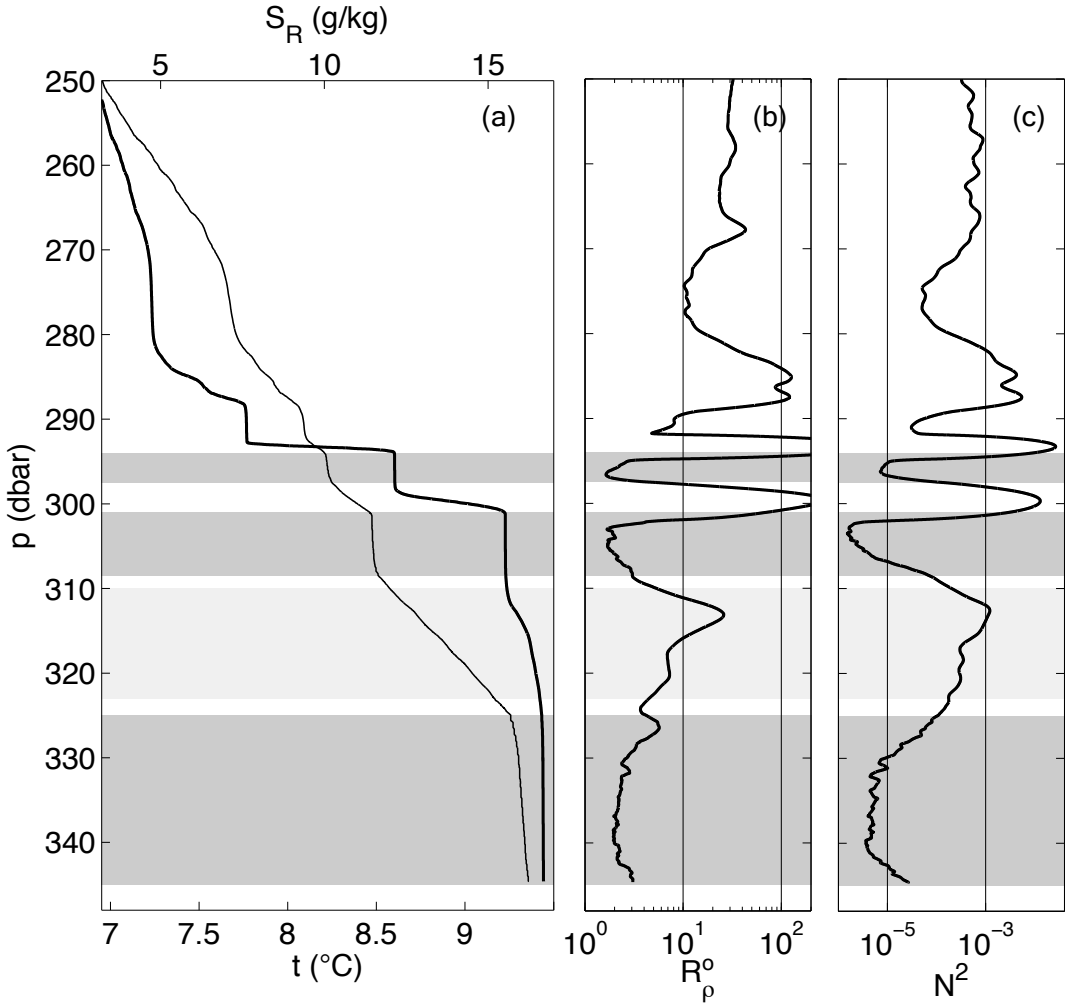

Figure 3.1 – Vertical profiles in the South Basin of Powell Lake. (a) In-situ temperature t (thin line) and Reference Salinity S_{R} (thick line) for the bottom 100 m. Profiles exhibit a large-scale step-like structure with double diffusive layers observed in the lowest three steps, shaded in dark grey. The light shaded region between 310-323 m is the one referenced in Section 3.3 which we use to estimate the steady state vertical heat flux. (b) Background density ratio R_ρ^o calculated from the t and S_{R} profiles shown in the left panel. (c) The corresponding large-scale buoyancy frequency N^2. Both b. and c. are smoothed using a 1 m running mean low-pass filter. All profiles are from station B06.

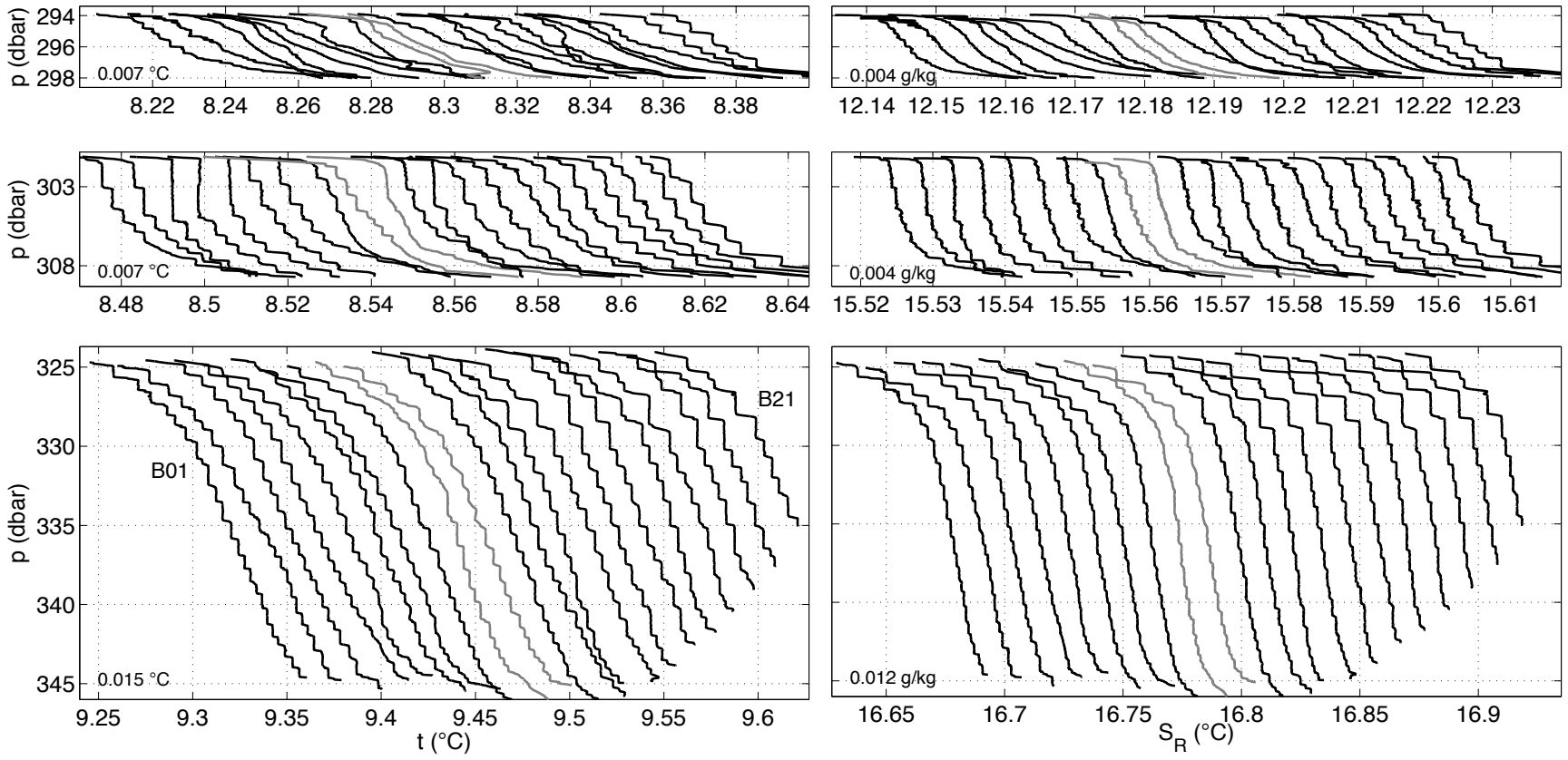

Figure 3.2 – Lateral transect of double diffusive layers in t (left) and S_{R} (right) at the three depths at which double diffusion is present. Profiles from left to right are from consecutive stations B01 to B21 as in Figure 2.1. The layering structure is least well established in the shallowest section and most clearly defined in the deepest portion. Each profile is horizontally offset from the previous by the value shown in the bottom left corner of each panel. The vertical scale is maintained throughout all six panels for easy comparison, and profiles from stations B09 and B10 are highlighted in grey. All profiles extend to within 1 m of the lake bottom.

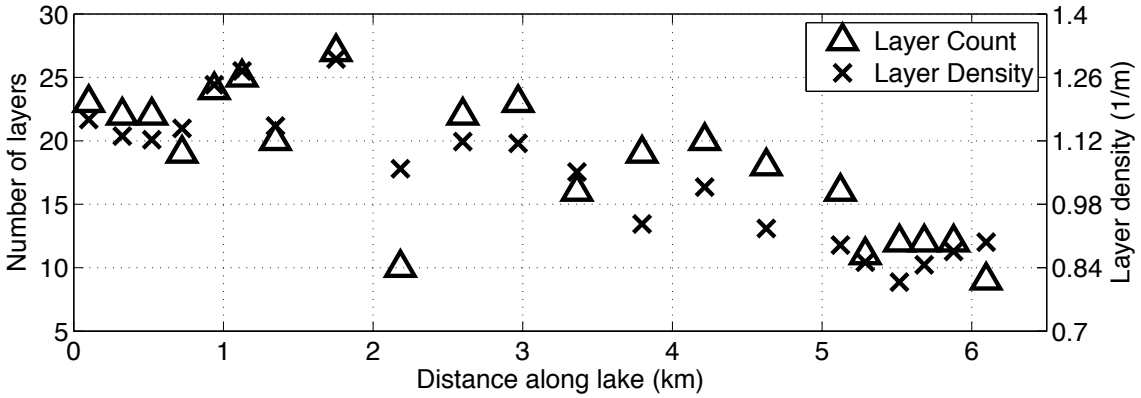

Figure 3.3 – Number of double diffusive layers below 324 m from south to north and the corresponding vertical layer density. Both decrease towards the northern end of the basin; the maximum number of layers observed is 27 and the minimum is 9, while the maximum layer density is 1.30 m^{-1} and the minimum is 0.81 m^{-1}.

In the deepest staircase, double diffusive layering is very well established and though temperature and salinity differences between layers are only on the order of one part in ten-thousand, we are able to clearly distinguish between layers over nearly the entire length of the basin. The majority of the 21 profiles shown in Figure 3.2 appear undisturbed; the profiles at stations B09 and B10 are exceptions to the rule as the staircase is not well-defined for these profiles between 327–335 m. This is a consistent signal over two days of measurements (second day of measurements not shown). The bottom bathymetry of the lake can be seen from the depth of the profiles, showing that the lake shallows by about 10 m towards the north end of the basin. As the lake shallows northward, there are fewer layers and the observed layers become about 40 percent larger on average so that the vertical layer density decreases from 1.25 to 0.84 m^{-1} (Figure 3.3). Note that the lake shallows more gradually southward and that our profiles do not extend far enough south to show this.

From 39 CTD casts, we obtained 756 individual observations of double diffusive layers and their dividing interfaces (Figure 3.4). The median mixed layer height is 0.71 m and the corresponding interquartile range (IQR) is 0.50–0.89 m; the median interface height in temperature is 0.18 m with an IQR of 0.13–0.24 m, and the median interface height in salinity is 0.17 m with an IQR of 0.11–0.24 m. On average, the temperature interface is 0.015 m or approximately 9% larger than the salinity interface. The median temperature difference between consecutive layers is 0.0036 °C and has an IQR of 0.0029–0.0047 °C, while the median salinity difference is 0.0013 g/kg with an IQR of 0.0011–0.0021 g/kg. We quote the median value rather than the arithmetic mean because the distributions are log-normal; however we also calculate the mean values (Table 3.1) for reference and intercomparisons with other studies.

The mixed layer and interface heights, and the temperature and salinity steps between

Parameter	Median	Mean	IQR
H (m)	0.67	0.71	0.50 - 0.89
h_T (m)	0.18	0.20	0.13 - 0.24
h_S (m)	0.17	0.19	0.11 - 0.24
Δt (°C)	0.0036	0.0043	0.0029 - 0.0047
ΔS_{R} (g/kg)	0.0013	0.0024	0.0011 - 0.0021
$h_T - h_S$ (m)	0.018	0.015	−0.02 - 0.05

Table 3.1 – Basic layer statistics, including layer height H, interface heights h_T and h_S, temperature and salinity steps Δt and ΔS_{R}, and interface size difference $h_T - h_S$. Shown for each variable are the median, the arithmetic mean, and the interquartile range (IQR).

layers all exhibit distinctive vertical structure. To characterize this, we create scatter-plots in depth (Figures 3.5 – 3.7) and calculate the average values within 1.75 m vertical bins. We choose this bin size because it is larger than nearly all observed layer heights, but small enough to provide at least 10 bins over the depth range of the staircase.

The interface heights are nearly constant, though they increase slightly from 0.15 m to 0.20 m towards the top of the staircase (Figure 3.5). The same is true of the difference $\delta h = h_T - h_S$ whose average remains consistently above zero and increases from approximately 0.010 m to 0.025 m towards the top (Figure 3.6b). There is considerable scatter in our observations of δh and a number of points fall below zero, indicating that for a portion of our observations the temperature interface is smaller than the salinity interface. This is unlikely as it would imply that the diffusive temperature interface is destroyed by mixing in the adjacent layers while the salinity interface remains intact. It is more probable that the scatter in our observations of δh reflects the limitation of our algorithm to characterize the boundary between the interface and the mixed layer. This is the case because the noise-to-signal ratio is quite high in the conductivity measurements. However, we maintain confidence in our instrument to resolve the vertical height of the interface in both temperature and conductivity: if, for example, a large number of salinity interfaces were too small for us to resolve, our observations of h_S would clump along a lower limit of 1.8 cm as set by the instrument resolution (Section 2.1), forming a dense collection of data points along the left-hand side of Figure 3.5b. Similarly, a large number of measurements below our detection limit would be reflected in the histograms of Figure 3.4a,b by a large number of observations at a lower limit. However, since the majority of data lie well above the instrument's resolution, it is unlikely that the size of either interface tends to be below our detection limit. Therefore, although there is substantial scatter in our observations of δh arising from the inherent difficulties of detecting the layer/interface boundary, we consider that the trend in our observations (given by the mean $\delta h \approx 1.5$ cm) accurately reflects the characteristics of the interfaces we observe.

The mixed layer height (Figure 3.6a) is distinctly larger towards the middle of the staircase, where $H \approx 1$ m, than it is towards the bottom and the top of the staircase where $H \approx 0.4$ m

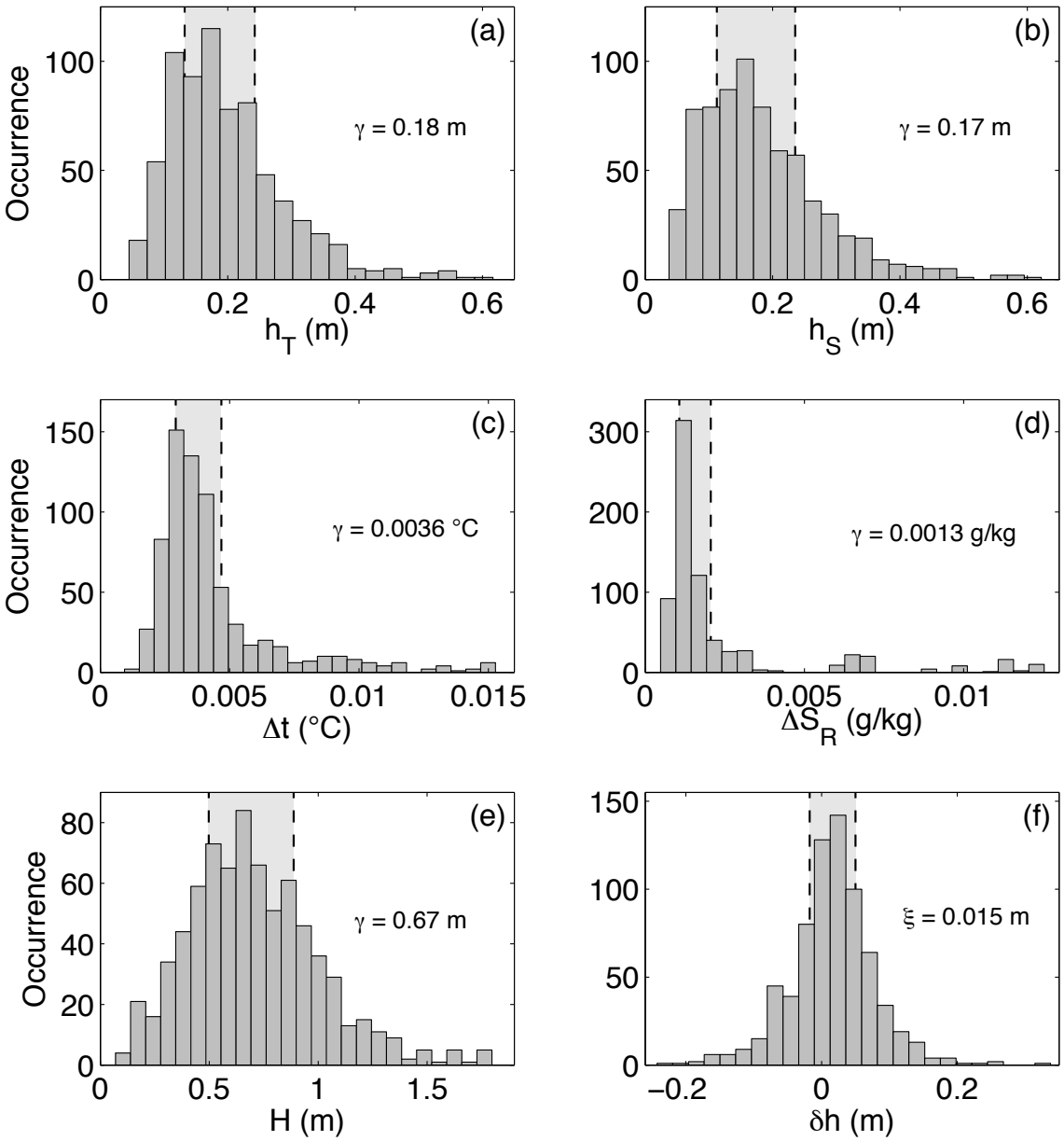

Figure 3.4 – Histograms of layer/interface characteristics, showing (a) temperature interface size, (b) salinity interface size, (c) temperature difference between consecutive layers, (d) salinity difference between consecutive layers, (e) layer height, and (f) difference between h_T and h_S. For each histogram, the lightly shaded area in the background between the dashed lines shows the interquartile range, and the median γ of the observable is given, except in (f) where the mean ξ is given.

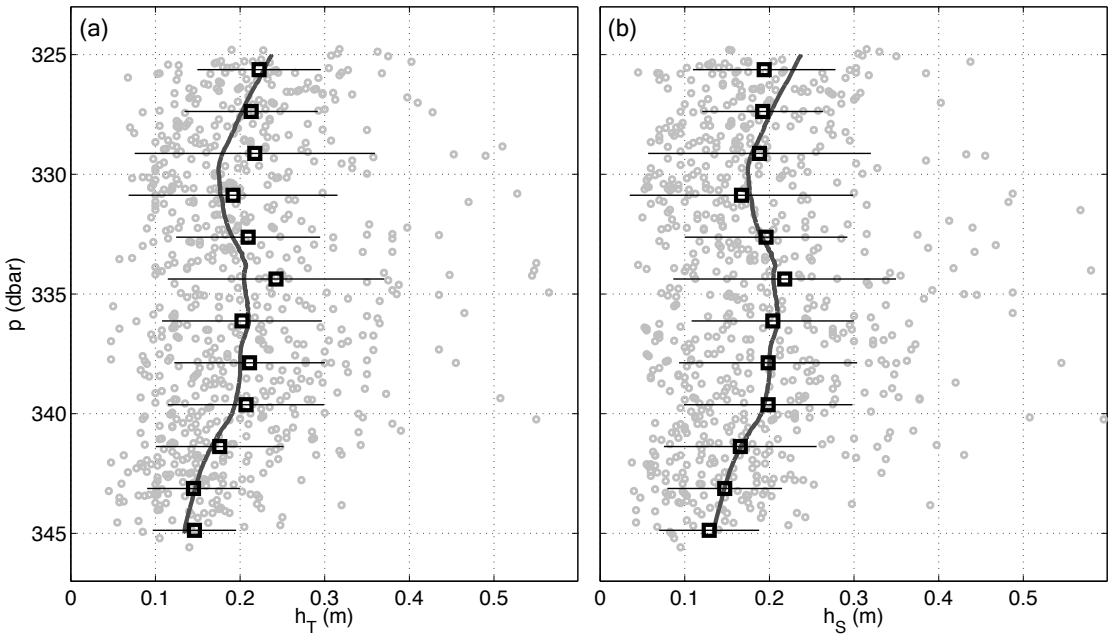

Figure 3.5 – Height of the double-diffusive interface in t (left) and S_{R} (right). Open grey circles represent individual interface observations, the dark line is a non-parametric loess curve (Cleveland, 1993) fitted to the observations, and the open squares are vertically binned averages using 1.75 m bins. Error bars show one standard deviation of the data that falls within each bin. The symbol and error bar conventions shown here are continued for Figures 3.6, 3.7 3.8, and 3.11.

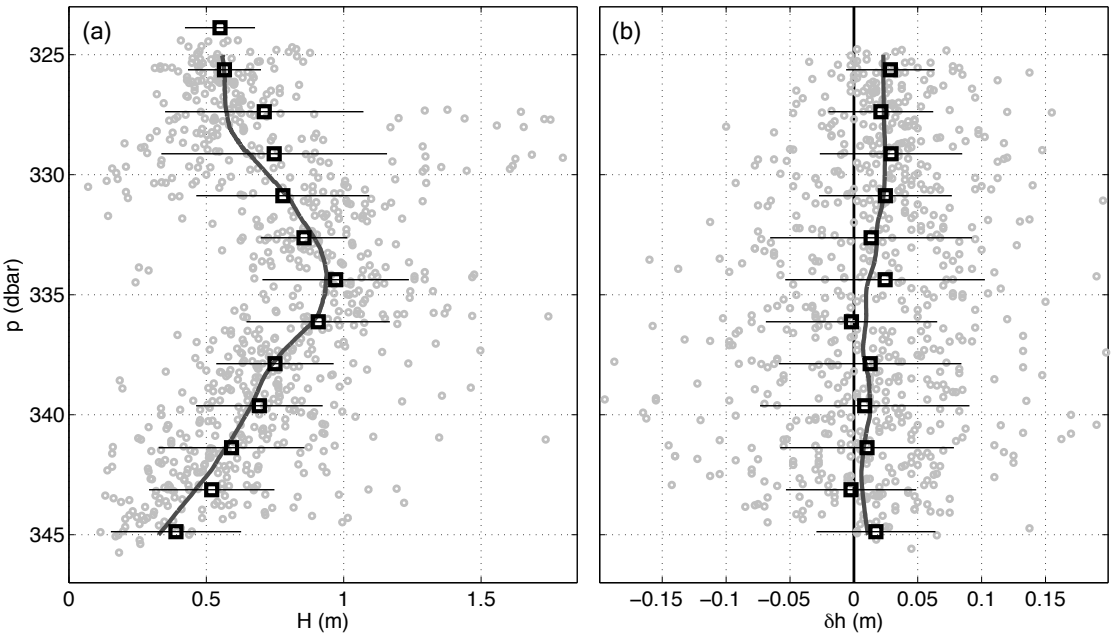

Figure 3.6 – (a) Layer height and (b) interface height difference. The measured double diffusive layer height H displays a clear vertical structure with larger values near the middle of the staircase. The difference δh between interface heights in t and S_{R} is constructed directly from Figure 3.5. We observe that h_T is about 9% larger than h_S throughout most of the staircase.

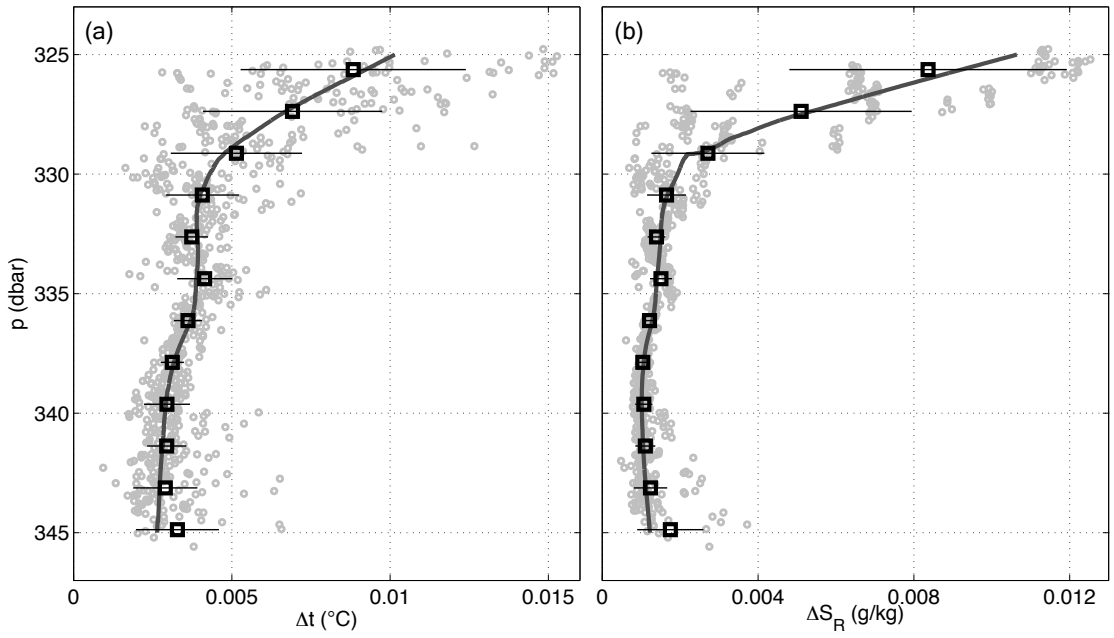

Figure 3.7 – (a) Temperature and (b) salinity steps between consecutive mixed layers, labelled Δt and ΔS_{R} respectively. Both remain fairly constant in the lower half of the staircase but increase strongly near the top. Measurements of ΔS_{R} across the two highest interfaces form distinctive clumps at approximately 0.006 g/kg and 0.011 g/kg which are not seen in the corresponding measurements of Δt.

and $H \approx 0.6$ m respectively. This is a consistent feature at all measurement stations. The temperature and salinity differences, Δt and ΔS_{R} display a different vertical structure which is likewise consistent across the length of the basin. Both become dramatically larger towards the top of the staircase (Figure 3.7). Δt increases approximately from 0.003 °C at 345 m, to 0.004 °C at 330 m, to 0.01 °C at 325 m depth. Similarly, ΔS_{R} increases approximately from 0.001 g/kg at 345 m, to 0.002 g/kg at 330 m, to as high as 0.012 g/kg at 325 m depth. The shallowest two interfaces span relatively much larger salinity steps than do the lower ones, resulting in two discrete clumps in the depth profile of ΔS_{R} (Figure 3.7b). Also notice that the scatter in observations of both Δt and ΔS_{R} is small, indicating that the size of the temperature and salinity steps are laterally consistent across the basin scale.

3.2 Interfacial Temperature Gradient

We calculate the temperature gradient ∇t in the interface using

$$\nabla t = \Delta t / h_T \tag{3.1}$$

We stress that this is the temperature gradient averaged over the interface, which will be systematically lower than the gradient at the centre of an idealized interface because of the transition zone at the boundary of the interface and adjacent mixed layers. Similar to other characteristic variables, the interfacial temperature gradient displays a clear vertical structure that is consistent across the basin (Figure 3.8a). The structure arises primarily because h_T remains nearly constant while Δt increases strongly towards the top of the staircase. Near 345 m depth the gradient is approximately 0.02 °C/m, decreases slightly around 340 m, and then begins to increase to a maximum of 0.04 °C/m at 325 m. The scatter at a given depth is primarily due to the relatively large scatter in measurements of h_T (Figure 3.5).

We calculate the density ratio across each interface using

$$R_\rho = \frac{\beta \Delta S_\mathrm{R}}{\alpha \Delta t} \tag{3.2}$$

where β and α are the average values within the interface and are calculated with respect to S_R and t. The vertical structure of R_ρ is similar to that of ∇t, lowest near the middle, and increasing gently towards the bottom and more strongly towards the top of the staircase (Figure 3.8b). Values range from 3 at the bottom, to 2 at 340 m depth, to approximately 6 at 325 m, and the scatter in the depth-averaged bins of the data is remarkably low. It is noteworthy that the shape of the vertical structure of ∇t reflects that of R_ρ; the linear correlation between the two variables is 0.50. Averaging the individual measurements across 1.75 m vertical bins yields a linear correlation of 0.95 (Figure 3.9).

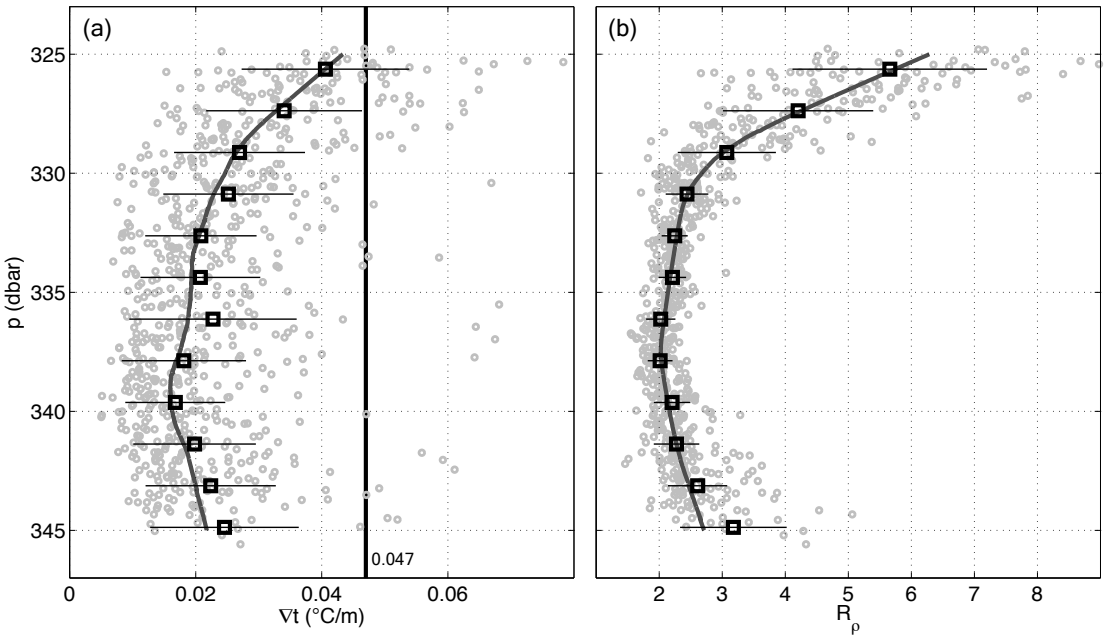

Figure 3.8 – (a) Average temperature gradient in the interface between layers. The vertical black line gives the steady state temperature gradient due to molecular diffusion as described in Section 3.3. (b) Density ratio across the interface, which is at its minimum in the middle of the staircase at $R_\rho \approx 2$ and is largest at the top of the staircase at $R_\rho \approx 6$.

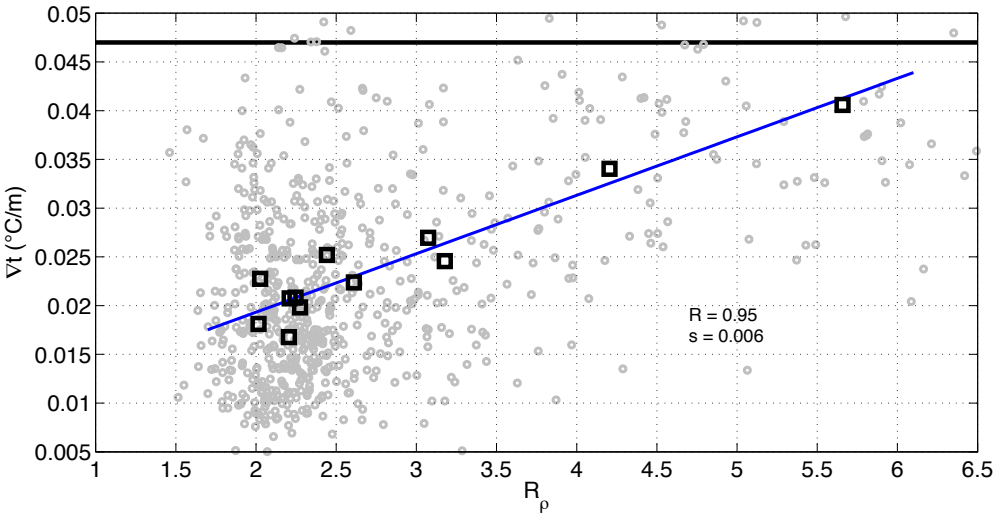

Figure 3.9 – Parametric plot in depth of ∇t against R_ρ, constructed from the data in Figure 3.8. At low values of R_ρ, the gradient in the interface is considerably lower than the steady state gradient (thick black line) we expect from molecular diffusion, while at higher values of R_ρ it approaches the steady state gradient. Open grey circles are the individual interface measurements, and open black squares are the 1.75 m vertically binned averages. This convention is continued for Figures 3.12 and 4.1. The depicted regression is that of the depth-binned data and has a linear correlation coefficient $R = 0.95$ and a slope $s = 0.006$.

3.3 Heat Fluxes

In order to test theories of double diffusive heat transport, independent estimates of the vertical heat flux are useful. Two such estimates are possible: first, Hyndman (1976) estimates the heat flux in the sediments of Powell Lake and finds a value of 27 ± 8 mW/m^2. If the heat budget of the saline layer is in a quasi-steady state, then the vertical heat flux through this portion of the watercolumn should be the same as the heat flux in the sediments, and for this reason we refer to it as the steady state heat flux. We consider the quasi-steady state assumption reasonable because the relic seawater in which we conduct our measurements has been quiescent and gradually heated since the most recent deglaciation (Sanderson et al., 1986). While it is true that the large-scale properties of the lake are still evolving slowly since salt continues to be lost to the surface through molecular diffusion, the rate at which this happens is much lower than that at which heat diffuses through the double diffusive region. A simple scaling of the diffusion equation (using t^* for time)

$$\frac{\partial T}{\partial t^*} = \kappa_T \frac{\partial^2 T}{\partial z^2} \tag{3.3}$$

suggests that the time scale for heat to diffuse through the bottom 50 m of the lake is approximately 600 years. This is substantially less than the age of the lake, giving the double-diffusive region sufficient time to reach a local thermal equilibrium. The quasi-steady state assumption is supported by a five-year series of CTD measurements (not shown) which show no apparent change in the large-scale structure of the temperature and salinity profiles in that time. If the saline layer were not in a quasi-steady state, we would expect to see a slight warming in the lower few meters of the lake, but this is not observed.

We gain a second estimate of the heat flux by assuming that vertical transport over the depths between 310–323 m is dominated by molecular diffusion. Across this depth range, the temperature profiles are almost perfectly linear and the strength of the temperature gradient is remarkably consistent at all observed stations along and across the lake (Figure 3.10). The gradient varies by less than one percent across all measured locations. Furthermore, we have no evidence to support the presence of significant turbulent energy at this depth. Both observations are consistent with the quiescence condition mentioned above and are discussed further in Section 4.3.

To calculate the mean temperature gradient between 310–323 m, we calculate the average gradient in thirteen one meter vertical bins at each of the 26 available measurement stations and then average over all stations. The mean temperature gradient calculated this way is 0.0472 ± 0.0003 °C/m, where the uncertainty is the standard error in the mean based on

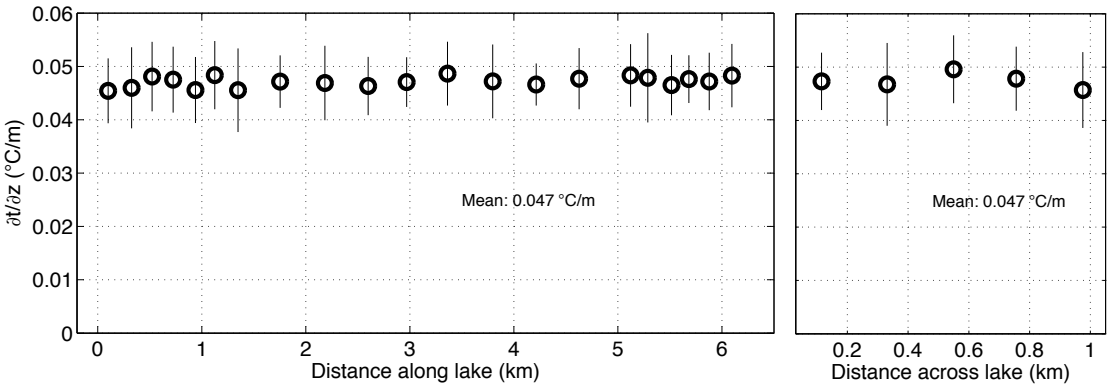

Figure 3.10 – Mean temperature gradient between 310 – 323 m depth, plotted as cross-sections along and across the South Basin. Error bars depict one standard deviation across thirteen one meter vertically averaged bins. The measured gradient is in excellent agreement with that expected from heat flux measurements by Hyndman (1976). It appears that vertical transport is dominated by molecular diffusion and that the temperature gradient over this depth is equilibrated to steady state.

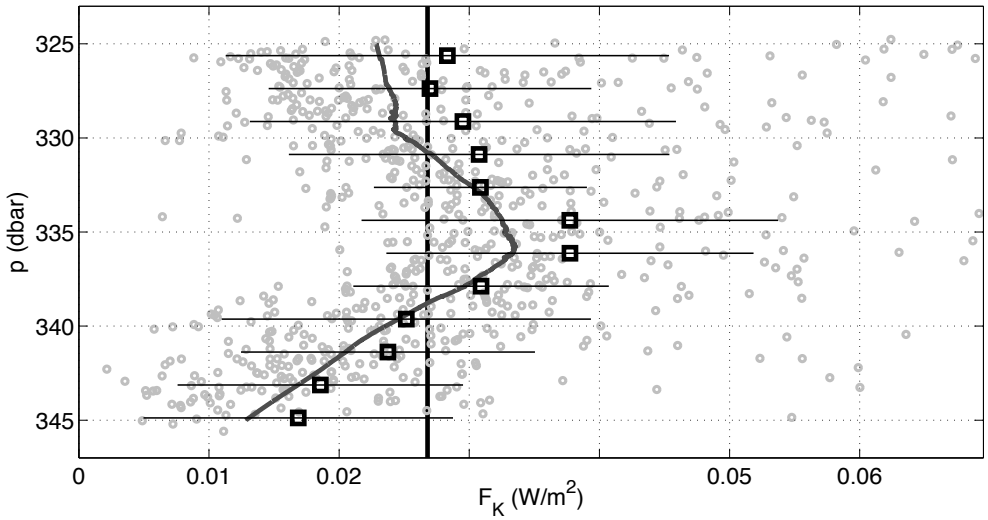

Figure 3.11 – Heat fluxes calculated using the 4/3 parameterization from Kelley (1990), given by Equation 1.15. The vertical black line is the steady state vertical heat flux deduced from Figure 3.10 and measured by Hyndman (1976). The parameterized heat fluxes appear accurate to within approximately a factor of two as evidenced by the vertical variation in F_K.

one standard deviation of all 26×13 bins. Using this value and taking

$$c_p = 4.1 \times 10^3 \text{ J/(kg °C)}, \quad \rho = 1012 \text{ kg/m}^3, \quad \kappa_T = 1.4 \times 10^{-7} \text{ m}^2\text{/s} \tag{3.4}$$

calculated at $t = 10$ °C and $S_\mathrm{R} = 15$ g/kg (Sharqawy et al., 2010), we use Equation 1.17 to estimate the vertical steady state heat flux through Powell Lake at 27 ± 1 mW/m^2.

The estimate of the vertical heat flux above the staircase agrees with that of the flux in the sediments below the staircase, and so because of steady state, our best estimate of the time-averaged vertical flux through the double-diffusive staircase is likewise 27 mW/m^2 at all depths within the staircase. We compare this estimate to the 4/3 parameterization of Kelley (1990) given by Equation 1.15 (Figure 3.11). We use values for c_p and κ_T as above, as well as $\nu = 1.3 \times 10^{-6}$ m^2/s also calculated at 10 °C and 15 g/kg, and $g = 9.8$ m/s^2. The parameterization calculated across each interface scatters about the steady state heat flux within about a factor of 2 and each 1.75 m bin has a standard deviation of approximately 0.01 mW/m^2. It has vertical structure resembling that of H (Figure 3.6a), tending to overestimate near the middle of the staircase ($F_K \approx 33$ mW/m^2) and underestimate near the top ($F_K \approx 22$ mW/m^2) and bottom ($F_K \approx 15$ mW/m^2).

While our two estimates of the vertical steady state heat flux are in agreement with each other, the interfacial temperature gradient we estimate using $\Delta t / h_T$ is on average not large enough to account for this flux by molecular diffusion alone (Figure 3.8a). Using Equation 1.17, the estimated heat flux of 27 ± 1 mW/m^2 should result in an interfacial temperature gradient of 0.047 ± 0.002 °C/m. The interfacial gradient we observe is less than half of this value over much of the staircase and only approaches it towards the top of the staircase where the density ratio also becomes large (Figure 3.8). This surprising result is discussed further in Section 4.5.

As outlined in Section 1.5, there has been considerable discussion regarding the correctness of the assumptions underlying the 4/3 parameterizations, specifically regarding the 1/3 exponent in the original scaling. Our measurements allow us to compare Nu and Ra directly to test for the exponent. In order to do this, we choose a subset of measurements over which R_ρ is approximately constant, in which case the scaling suggests that $Nu \propto Ra^n$ directly (from Equation 1.9), where n is now a generalized exponent. We include all interfaces across which the density ratio falls in the range $1.5 < R_\rho < 2.5$ and plot $\log(Nu)$ against $\log(Ra)$ (Figure 3.12); the exponent n is then given by the slope of the linear regression. In total, 441 or 58% of the observed interfaces fall within the prescribed range of R_ρ. To calculate Nu and Ra, we use the layer height above the interface as a length-scale and the estimated steady state heat flux of 27 mW/m^2. The logarithms are both calculated at base 10.

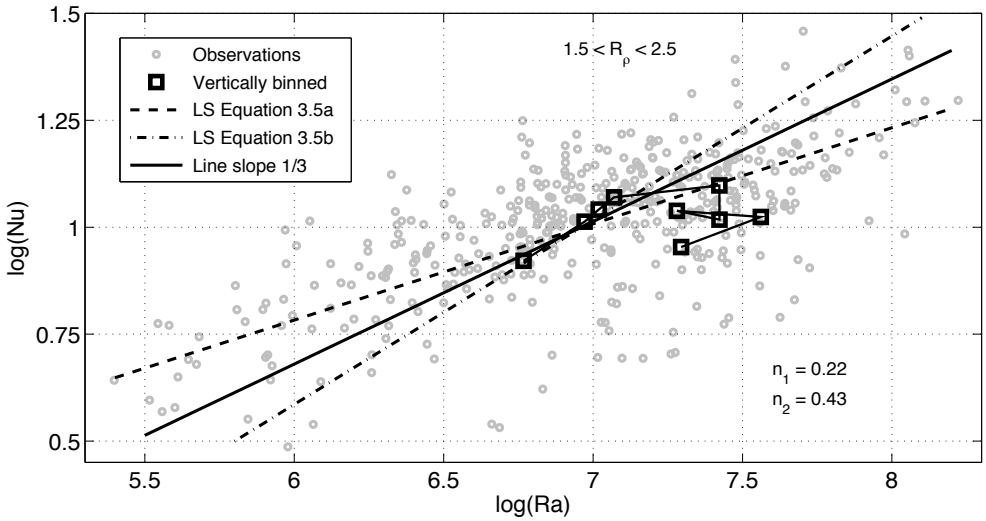

Figure 3.12 – A direct test of the scaling $Nu = f_1(R_\rho)Ra^n$. We use a subset of the available data over which R_ρ does not vary much so that the factor f_1 is approximately constant. Two linear least squares (LS) regressions incorporating distinct error structures, as described in the text, give that $0.22 \leq n \leq 0.43$. A line with slope 1/3 is shown for comparison. The vertically averaged bins of the data are connected by a thin line, showing the progression from deepest (with lowest Ra) to shallowest. Note that the vertically averaged bins do not follow an obvious linear trend as would be expected from a scaling of the form $Nu \propto Ra^n$, but that they deviate systematically from this power law.

A standard least squares regression minimizes the sum of the squared measurement errors along the vertical axis. It assumes that there is no measurement error along the horizontal axis. However, in our observations of Nu and Ra, both variables contain an associated measurement error and it is incorrect to associate the entire uncertainty to only one variable. Consequently, we calculate the linear regression to the data shown in Figure 3.12 in two ways. Using the least squares method, we perform a regression assuming each error structure independently:

$$\log(Nu) = n_1 \left(\log(Ra) + \delta \log(Ra)\right) \tag{3.5a}$$

$$\log(Ra) = \frac{1}{n_2} \left(\log(Nu) + \delta \log(Nu)\right) \tag{3.5b}$$

where the δ term is the measurement error associated with the respective variable. The first model assumes that all the uncertainty is contained in measurement errors of Ra; the second assumes that the entire uncertainity results from measurement errors in Nu. The two methods produce substantially different estimates for the exponent, giving $n_1 = 0.22$ and $n_2 = 0.43$, and these values can be taken as lower and upper bounds for an ideal regression. If the form of the scaling is correct, then the true exponent lies somewhere between these two values, and choosing $n = 1/3$ visually matches the trend in the data reasonably well. The strength of the linear correlation between $\log(Nu)$ and $\log(Ra)$ for the range $1.5 < R_\rho < 2.5$ is 0.72.

However, notice that the depth-averaged bins of the data do not follow a purely linear trend. The deepest four bins do appear linear with a slope $n > 1/3$, but the shallowest five bins (with $Ra > 10^{7.2}$) systematically deviate from a linear trend. Taken together, the depth-averaged bins form a convex shape that does not follow a power law of the form $Nu \propto Ra^n$. This result is surprising because the binning process tends to remove scatter and extract the underlying trend from the raw observations; the implication is that a scaling of the form $Nu \propto Ra^n$ is fundamentally inconsistent with our observations. This result and its implications are discussed further in Sections 4.3 and 4.4.

3.4 TS Diagrams and Layer Coherence

The mixed layers of the double diffusive staircase in Powell Lake group in clusters similar to those observed in the Canada Basin of the Arctic (Timmermans et al., 2008) when plotted in temperature-salinity space (Figure 3.13). This indicates that individual layers are coherent and can be traced over the scale of the basin. A layer that has a vertical scale height of 1 m and a lateral scale length of 10 km has an aspect ratio of 10^4. Furthermore, as our measurements span two days, we can say that layers remain coherent for at least that period. The three shallowest layers are notable exceptions. For these, the temperature-salinity properties appear to split approximately halfway along the basin. The salinity properties in particular seem to diverge: the upper two layers tend to be less saline in the southern portion of the basin and the third layer tends to be more saline in the southern portion of the basin.

The other layers appear to maintain relatively similar lateral gradients and are systematically saltier and cooler, and therefore heavier, towards the northern end of the basin. However, gradients are extremely small: they are order 10^{-6} °C/m and 10^{-5} (g/kg)/m in temperature and salinity respectively. The deepest few layers become difficult to distinguish on the diagram because the salinity difference between layers is no longer larger than the salinity difference in one layer over the length of the basin. Timmermans et al. define a lateral density ratio $R_{\rho x}$ to characterize the along-layer gradients:

$$R_{\rho x} = \frac{\beta S_x}{\alpha \Theta_x} \tag{3.6}$$

which is given by the inverse of the slope of the clusters in Figure 3.13. Θ is conservative temperature, chosen here in place of t because mixed layers are thought to be convective (see Section 2.2). We calculate the slope for seven of the most readily identifiable clusters and so find a lateral density ratio of $R_{\rho x} = -0.46 \pm 0.18$.

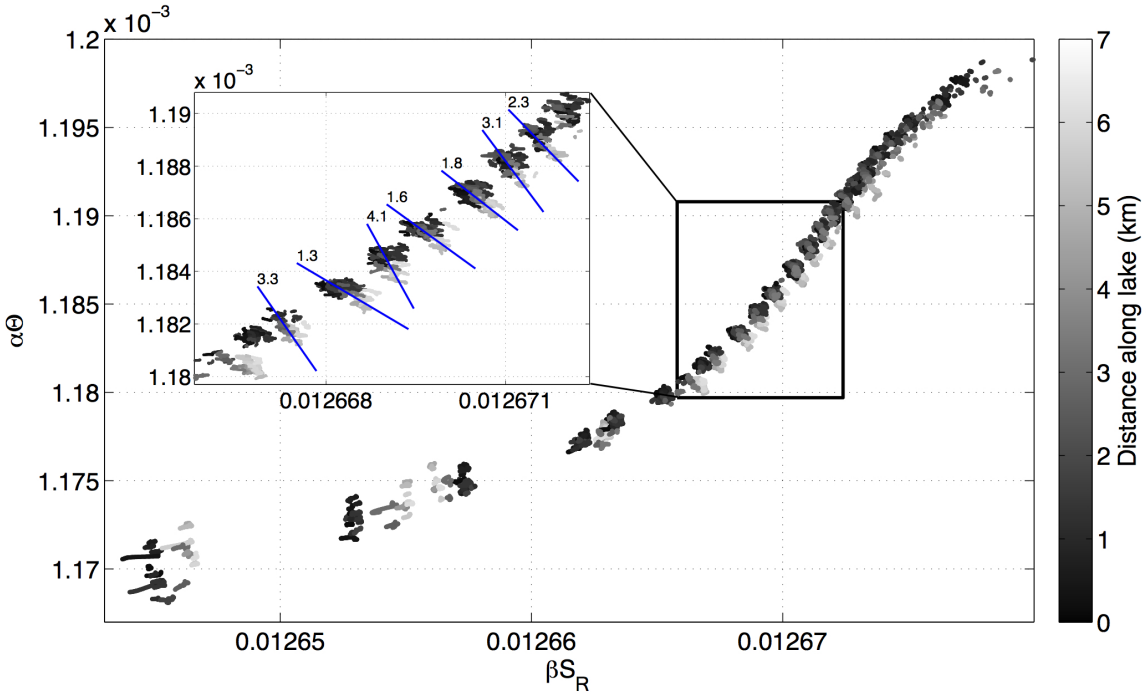

Figure 3.13 – Temperature-salinity diagram of double diffusive mixed layers, not including measurements of the interfaces. Θ and S_R are non-dimensionalized by α and β respectively. Layers group along distinctive clumps indicating that they are coherent over the basin scale. They consistently exhibit horizontal gradients in both variables, and the magnitude of the slope for a few layer groupings is shown in the inset.

Chapter 4

Discussion

4.1 Large-scale properties

The gross features of the temperature and salinity structure of the South Basin of Powell Lake are described well by a simple one-dimensional diffusion model in which the eddy diffusivity decreases exponentially with depth (Sanderson et al., 1986). The difference in the shape of the two profiles arises because of the differing boundary conditions in T and S. The temperature profile is continually forced by a geothermal heat flux below while losing heat into the mixed fresh layer above; this results in a quasi-steady state in which the temperature profile changes only little with time after the first 5000 years. The salinity budget on the other hand is necessarily negative as salt is continually lost into the mixed layer, slowly depleting the salt reservoir in the deep water.

The large-scale step structure in the temperature and salinity profiles (Figure 3.1) is not reproduced in the one dimensional diffusion model of Sanderson et al. (1986). Similar large-scale steps are observed in Lake Kivu where the steps are thought to be caused by the inflow of subaquatic springs at various depths (Schmid et al., 2010). In Powell Lake there are no obvious indications of subaquatic inflows (for example, consistent mid-depth temperature maxima); futhermore, substantial inflows below the halocline would contribute to flushing the salt from the deep layer more rapidly than is accounted for by the simple diffusion model of Sanderson et al. (1986). Since the model is able to account for the bulk of the salt budget over the last 11,000 years by diffusion, there is strong indication that there are no substantial inflows below the halocline. Consequently, it appears unlikely that the large-scale step structure in Powell Lake results from the effect of subaquatic inflows.

Alternatively, it is conceivable that the steps are related to the hypsography of the lake; unfortunately, the only available bathymetry information for Powell Lake is from Mathews (1962) which is too scarce to produce a well-resolved hypsography. A more thorough study

of depth soundings is required to create isobaths at a sufficient resolution to produce a precise hypsography below 250 m depth. However, echo sounding transects carried out during the course of numerous trips over five years do not indicate that there are well defined steps in the bathymetry of the lake (Pawlowicz, personal communication).

Lastly, a possibility that has not been explored in previous studies is that the large-scale steps are themselves related to the double diffusive layers found within them. Perhaps the low-gradient regions develop because of the formation of double diffusive layers which more effectively transport heat and salt through the watercolumn. This idea would explain why double diffusive layers are found only in the low-gradient regions of the profiles. It fails to explain why double diffusive convection becomes active in some regions of the watercolumn but not in others. In this scenario, the current profiles of R_ρ^o and N^2 are of little value in explaining the formation of double diffusive layers as these would have had a different vertical structure before layering developed than they do currently.

The location of double diffusive layering in Powell Lake generally follows the approximate criterium that $1 < R_\rho^o < 6$, but this is not sufficient to explain all the observed structure. For example, there is some overlap in the values of R_ρ^o that are observed between 310–323 m where there is apparently no double diffusion present and below 324 m where double diffusive layering is well established (Figure 3.1). The overlap exists primarily at the intersection of the two regions: approaching the top of the staircase from below, the background density ratio decreases at 324 m to a value of 4, before increasing again to a value of 8 at 320 m. Yet, there appears to be no double diffusive instability over this depth range. It is noteworthy that the large-scale instability N^2 does not exhibit a similar overlap in values between the double diffusive and the stable regions, suggesting that perhaps double diffusive layering can additionally be governed by the large-scale stability.

Considering only the background density ratio also does not explain why layering is very well established below 324 m depth while it appears slightly more disturbed in the higher double diffusive region between 301–309 m, and can hardly be seen at all in the shallowest double diffusive region between 294–298 m. The most likely explanation for the increasingly disturbed staircases in the shallower regions is that eddy diffusivities are no longer negligibly small. It is likely that some turbulence propagates from the surface to disturb the higher two staircases. In the modelling scheme of Sanderson et al. (1986), eddy diffusivity is comparable to molecular diffusivity at the bottom but increases exponentially towards shallower depths.

4.2 Comparison of Layer Characteristics

The properties of the double diffusive layers in Powell Lake are not unlike those found in other locations (Table 4.1). The layer height in Powell Lake ranges approximately between 0.2–1.5 m; in Lake Kivu it ranges between 0.1–0.8 m (Schmid et al., 2010); in Lake Nyos it ranges between 0.2–1.7 m (Schmid et al., 2004); and in the Canada Basin of the Arctic it ranges approximately between 1.0–5.0 m (Timmermans et al., 2008). That is, in all cases the layers tend to have a scale height of about 10 cm to 1 m. It is not clear what determines the layer height in a double diffusive staircase; a parameterization for H does exist (Kelley, 1984) and is based on the large scale stability N^2, but for Powell Lake this parameterization calculates layer heights that scatter between 1.5–4.0 m which are too large to accurately describe the observed layer heights.

The interface height is remarkably similar in all the cases described above. The temperature interface height h_T varies approximately between 0.1–0.4 m in Powell Lake, 0.1–0.3 m in Lake Kivu, and 0.1–0.3 m in Lake Nyos. No exact interface height information is available for the Canada Basin staircase; however both Padman and Dillon (1987) and Timmermans et al. (2008) suggest that the interfaces are roughly 0.10 m high. It is qualitatively understood that the interface height is likely controlled by (buoyancy driven) separation of the interface's unstable boundary layer or by convection in the adjacent mixed layers (Carpenter et al., 2012; Linden and Shirtcliffe, 1978; Padman and Dillon, 1987), but no quantitative analysis has successfully predicted the observed interface heights in geophysical situations.

Heat fluxes vary by an order of magnitude between the five studies described here. In Powell Lake, we estimate that the vertical heat flux is 27 mW/m^2 (Section 3.3). From the above references, the vertical heat fluxes in Lake Kivu are approximately 10–100 mW/m^2, while those in Lake Nyos are roughly 100–600 mW/m^2. Padman and Dillon (1987) estimate the vertical heat flux through most of the staircase in the Canada Basin to be about 40–70 mW/m^2, while Timmermans et al. (2008) estimate the flux to be 50–300 mW/m^2. Note that of the above estimates, only the one in Powell Lake does not rely on either a 4/3 flux parameterization or on the assumption that interfaces between layers are controlled by molecular diffusion (though the study in Lake Nyos does make a comparison to an independent estimate from a heat budget calculation).

The observed temperature differences between consecutive layers likewise vary by an order of magnitude between the above sites. Those in Powell Lake and Lake Kivu are quite similar, with temperature differences that vary between 0.001–0.015 °C and 0.001–0.018 °C respectively. In Lake Nyos, Δt tends to be higher and is observed in the range 0.015–0.047 °C. In the Canada Basin, Padman and Dillon (1987) find temperature differences that range between about 0.004–0.012 °C, while Timmermans et al. (2008) find $\Delta t \approx 0.04$ °C. Salinity differences are only available for the Canada Basin, where Padman and Dillon (1987) find

	R_ρ	H (m)	h_T (m)	Δt (°C)	ΔS_R (g/kg)	F_H (mW/m^2)
Powell Lake	1.5–8	0.2–1.5	0.1–0.4	0.001–0.015	0.001–0.002	27
Lake Kivu Schmid et al. (2010)	–	0.1–0.8	0.1–0.3	0.001–0.018	–	10–100
Lake Nyos Schmid et al. (2004)	–	0.2–1.7	0.1–0.3	0.015–0.047	–	100–600
CB – Padman and Dillon (1987)	4–5	1.2–3.0	~ 0.1	0.004–0.012	0.001–0.005	40–70
CB – Timmermans et al. (2008)	2–7	1.0–5.0	~ 0.1	~ 0.04	~ 0.014	50–300

Table 4.1 – An overview of double diffusive parameters from five distinct studies, comparing Powell Lake, Lake Kivu, Lake Nyos, and the Canada Basin (CB) of the Arctic.

$\Delta S_\mathrm{R} \approx 0.001$–$0.005$ g/kg and Timmermans et al. (2008) find $\Delta S_\mathrm{R} \approx 0.014$ g/kg. Interfacial density ratios are therefore also available only for the Canada Basin where Padman and Dillon (1987) find $R_\rho \approx 4$–5 and Timmermans et al. (2008) find an approximate range $2 < R_\rho < 7$. The latter is very similar to the range of density ratios we observe in Powell Lake, which is $1.5 < R_\rho < 8$.

Lastly, we find that layers in Powell Lake form clumps in T–S space similar to those in the Canada Basin described by Timmermans et al. (2008). In both cases, these clumps cross isopycnals in a systematic manner; however, the lateral density ratio calculated from these groups has a larger magnitude and varies less in the Canada Basin ($R_{\rho x} = -3.7 \pm 0.9$) than it does in Powell Lake ($R_{\rho x} = -0.46 \pm 0.18$).

4.3 Heat Fluxes

Our approach from Section 3.3 of estimating the vertical heat flux by considering that transport between 310–323 m is dominated by molecular diffusion rests on the assumptions that the lake is quiescent at this depth and that the system can be accurately represented by a one-dimensional model. This requires that the eddy diffusivity and lateral divergence both be negligibly small. These are strong conditions which are generally not true in the ocean, but our observations support the assumption that they do hold in Powell Lake.

Firstly, the presence of a permanent anoxic boundary at 130 m depth confirms that there is no large-scale overturning circulation in the South Basin. This idea is supported by the presence of the 11,000 year old salt layer which likewise indicates that turbulent mixing across the halocline is minimal and that eddy diffusivites in the salt layer are extremely small. The one-dimensional diffusion model of Sanderson et al. (1986) is largely able to

account for the salt lost from the saline layer over the past 11,000 years by assuming a diffusivity profile in which eddy diffusivity is comparable to molecular diffusivity at depth. Furthermore, it is very unlikely that there are subaquatic inflows below the halocline as these would contribute to flushing the salt from the basin. And while there are seiching motions in the lake which may contribute to enhanced mixing at the boundaries, the observed vertical displacement from comparing the 39 CTD casts is small and has a height of approximately one meter. It is unlikely that seiching motions produce substantial mixing at the boundaries because we do not observe a large mixed boundary layer at the bottom of the lake – the double diffusive staircase is typically undisturbed to within 1 meter of the lake bottom.

Perhaps the most compelling evidence in support of the quiescence and one-dimensionality argument is the observed lateral homogeneity of the large-scale properties, specifically that of the temperature gradient between 310–323 m. It is unlikely that the temperature gradient here would be constant within less than 1 percent across the entire basin in all measured profiles if localized mixing processes were significant contributors to the vertical transport. The near linearity of the temperature gradient is also consistent with the quasi-steady state condition and with the physics of molecular diffusion. Lastly, it is remarkable that the flux estimate obtained from this gradient is exactly that estimated by Hyndman (1976) in the sediments of the lake. This result too is entirely consistent with the quasi-steady state condition.

Implicit in the one-dimensionality argument is the assumption that heating from the basin sides can be neglected in the analysis. The net geothermal heat input to the basin is proportional to the total surface area of the bathymetry, and the net integrated heat transport must be vertically upwards in a symmetric basin. Because we consider only the bottom 50 m of the lake and because the lake has a classic fjord-like bathymetry with very steep sides and a relatively flat bottom, we can approximate the longitudinal cross-section below 300 m depth as an open rectangle 2 km wide and 50 m high on either side. This implies that the side walls of the basin contribute no more than 5% to the total heat budget of the lower staircase if the basin sides and bottom are uniformly heated. If we consider shallower depths, it may be necessary to include the effects of side-wall heating as the relative proportion of the influence of the sides of our model box increases.

Previous observational studies (Timmermans et al., 2008; Schmid et al., 2010) compare the fluxes calculated by the 4/3 parameterization to that calculated using the gradient in the interface between layers; this assumes that molecular diffusion is the single dominant transport process in the interface and does not account for entrainment that may occur across the interface from rising and falling convective plumes. We are able to obtain two separate (and consistent) measures of the heat flux which rely neither on the assumptions inherent in the flux parameterizations nor on the assumption that interfaces are undisturbed by turbulent processes. This allows us to characterize the accuracy of the 4/3 parameterizations

with a confidence that has not been possible in previous studies, and it allows us to test for the diffusive nature of the interface in a natural system.

The instantaneous heat flux from layer-to-layer may not be identical to the large scale temporally and spatially averaged flux since laboratory work (Marmorino and Caldwell, 1976) and direct numerical simulation (Carpenter et al., 2012; Noguchi and Niino, 2010b) emphasize the dynamic nature of double diffusive layering. However, integrated over time or space, we expect double diffusive fluxes to agree with the steady state heat flux. Therefore, the factor of approximately two that describes the difference in the bin-averages of the heat flux parameterization from the steady state flux (Figure 3.11) characterizes the parameterization's ability to estimate the actual flux. If the quasi-steady state condition holds, then the vertical structure in the parameterized heat flux reflects a systematic bias from the actual flux which could vary with either R_ρ or Ra.

This opens the door to a discussion on the correctness of the current double diffusive flux scaling. There are two possibilities that may be addressed regarding this topic. The first approach assumes the correctness of the scaling $Nu = f_1(R_\rho)\, Ra^n$. Originally, n was chosen to be $1/3$ because this removes the dependence on H, but more recent work has shown that other exponents may produce better results (Kelley, 1990). From our observations (Figure 3.12), it is difficult to ascertain whether a different exponent would produce better results; the exponent may lie anywhere between 0.22 and 0.43, and an exponent of $1/3$ would explain the observations as well as any within these limits and over the range $1.5 < R_\rho < 2.5$.

One difficulty of using an exponent other than $1/3$ is that this breaks the assumption on which the scaling was originally built, that the fluxes should be independent of H. This is an inconsistency which needs to be explained if the scaling continues to be used. However, regardless of which exponent is chosen for the above scaling, a more fundamental question is highlighted by our observations. Notice that the vertically averaged data in Figure 3.12 do not randomly scatter about a linear regression; rather, they seem to form a convex shape if traced from deepest to shallowest. This implies that the observations systematically deviate from the proposed power law scaling and no constant value of n would be able to capture this trend. This systematic deviation from a power law is the reason for the observed bias in the vertically averaged heat flux parameterization shown in Figure 3.11. The inability of the current scaling to account for this bias indicates that perhaps a new scaling may better represent the physics of the phenomenon. This is the second possibility which should be considered when discussing the correctness of double diffusive flux parameterizations.

4.4 New Scaling Observations

While we do not fully develop a new theoretical scaling here, we at least suggest that a new scaling may be appropriate. In the original development of the current scaling, Ra was chosen as the governing parameter in Equation 1.8 in analogy to single-component thermal convection. However, this is partially arbitrary as R_ρ may equally well have been chosen as the governing parameter (Turner, 1973). In hindsight, it may be more reasonable to choose R_ρ as the governing parameter because this directly incorporates the stabilizing effect of the salt gradient into the scaling; by choosing Ra as the governing parameter, the effect of the salt gradient on the heat flux must always be included through an empirical function of R_ρ. Furthermore, Ra can vary strongly in a particular system while R_ρ typically varies only over a much narrower range. Even in a simple system such as Powell Lake where the steady state heat flux can be taken as constant, the Rayleigh number varies by nearly three orders of magnitude because of the observed variation in H (Figure 3.12).

An alternate plausible form for Equation 1.8 with R_ρ as the governing parameter is

$$Nu \propto R_\rho^{-1} \tag{4.1}$$

and we find that this relation is remarkably successful in describing our observations (Figure 4.1). The observed dimensionless proportionality constant is $m = 29$, so that from our observations

$$Nu = 29\, R_\rho^{-1} \tag{4.2}$$

It is natural to see some scatter in the individual layer/interface measurements (open circles) because we use the steady state flux to calculate Nu even though the individual interface fluxes are at steady state only when averaged over a number of measurements. However, we do expect the vertically binned averages (open squares) to reflect the steady state flux, and these follow Equation 4.2 remarkably well, much better than in the conventional Nu–Ra scaling. Compare Figures 3.12 and 4.1.

A scaling of the form $Nu \propto R_\rho^{-1}$, if verified by other observations, has a number of theoretical advantages over the Nu–Ra scaling. Firstly, it directly accounts for the stabilizing effect of the salt gradient. It is possible to see this more clearly if, following Turner (1973), we define a salinity Rayleigh number

$$Rs = \frac{g\beta\Delta S H^3}{\nu\kappa_T} \tag{4.3}$$

which characterizes the negative buoyancy of the salinity contribution. Then

$$R_\rho = Rs/Ra \tag{4.4}$$

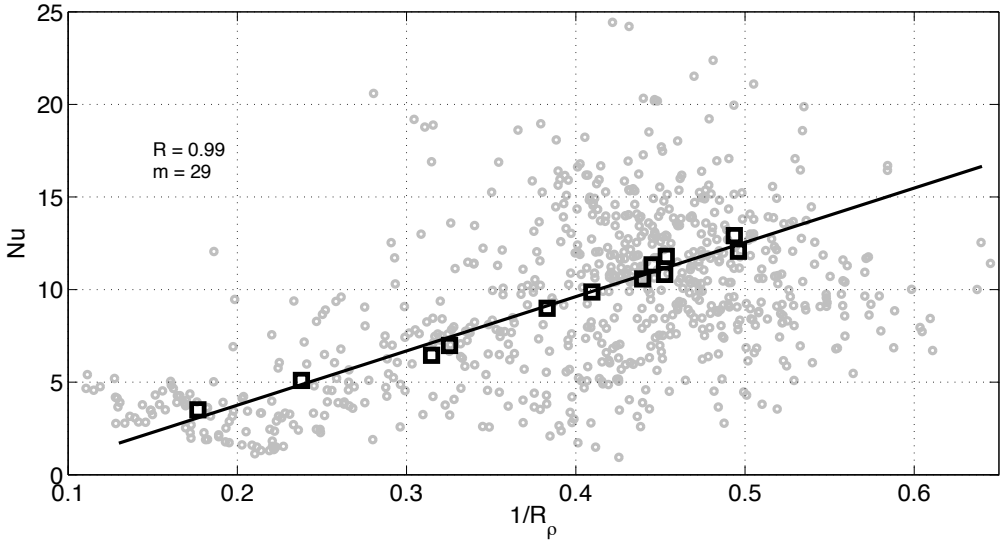

Figure 4.1 – Parametric plot in depth showing that $Nu \propto 1/R_\rho$ in our observations. The relationship shown here is evidently much stronger than that of the traditional scaling $Nu \propto Ra^{1/3}$ which is given in Figure 3.12. Shown also are the correlation R between the depth averaged bins as well as the slope m of the least squares fit to the binned data.

and Equation 4.1 becomes

$$Nu \propto Ra/Rs \tag{4.5}$$

Incidentally, it is now easy to see that a scaling of this form would not necessarily require an empirically determined function similar to $f_1(R_\rho)$. It already inherently includes two physically relevant non-dimensional parameters.

Secondly, a scaling of the form $Nu \propto R_\rho^{-1}$ is independent of variations in the individual layer characteristics and allows for flux calculations based solely on the large-scale temperature and salinity gradients. In order to see this, we rewrite Equation 4.2 by substituting the definitions of the dimensionless variables and keeping the proportionality constant m in its generalized form:

$$\frac{HF_H}{\rho c_p \kappa_T \Delta T} = m \, \frac{\alpha \Delta T}{\beta \Delta S} \tag{4.6}$$

This can in turn be rewritten as

$$\frac{F_H}{\rho c_p \kappa_T} \, \frac{1}{(\Delta T/H)} = m \, \frac{\alpha}{\beta} \, \frac{(\Delta T/H)}{(\Delta S/H)} \tag{4.7}$$

If the background stratification is fixed, only the ratios $\Delta T/H$ and $\Delta S/H$ are important in determining the shape of the temperature and salinity profiles. However, notice that dividing smooth temperature and salinity profiles into steps of arbitrary size leaves these ratios unchanged (Figure 4.2). Consequently, variations in individual layer properties do not affect Equation 4.1 as long as the background stratification does not change.

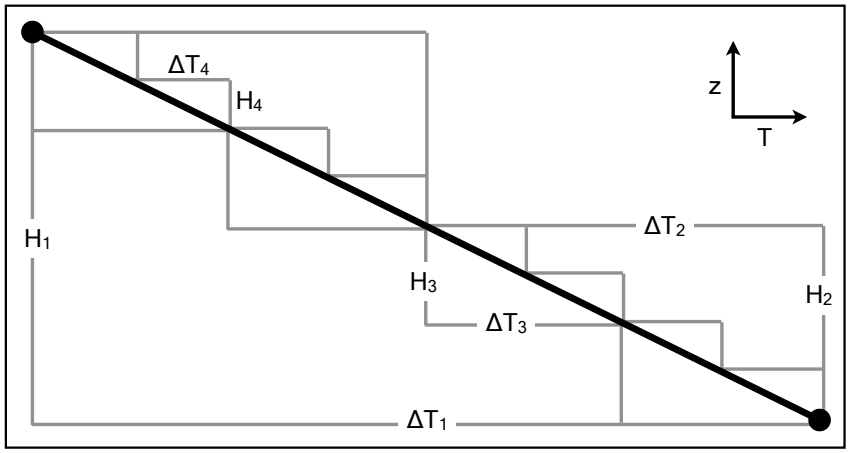

Figure 4.2 – Schematic depicting the invariance of $\Delta T/H$. Dividing a fixed background temperature profile (thick black line) into steps of arbitrary size leaves the ratio $\Delta T/H$ unchanged. In this example, the value of $\Delta T_i/H_i$ is the same for $i = 1, 2, 3, 4$. The description for a fixed salinity profile would be analogous.

Isolating F_H by rearranging Equation 4.6 gives

$$F_H = \rho c_p \kappa_T \frac{\Delta T}{H} \frac{m}{R_\rho} \tag{4.8}$$

Exploiting the demonstrated invariance of Equation 4.1, the discrete ratios become derivatives in the limit as H, ΔT and ΔS become small:

$$\frac{\Delta T}{H} \longrightarrow \frac{\partial T}{\partial z} \quad \text{and} \quad R_\rho \longrightarrow R_\rho^o$$

Here, the vertical derivative is now that of the large-scale temperature profile. With this information, the expression for the double diffusive heat flux becomes remarkably similar to that of a regular diffusive flux, only scaled by m and R_ρ^o:

$$F_H = \rho c_p \kappa_T \frac{\partial T}{\partial z} \frac{m}{R_\rho^o} \tag{4.9}$$

To make this more clear, we can define an effective diffusion heat flux in analogy to single component molecular diffusion:

$$F_{HM} = \rho c_p \kappa_T \frac{\partial T}{\partial z} \tag{4.10}$$

The double diffusive heat flux is then simply given by

$$F_H = F_{HM} \frac{m}{R_\rho^o} \tag{4.11}$$

Notice that Equation 4.9 relies only on the large scale properties of the background stratification and not on the individual layer characteristics of the double diffusive staircase.

However, the above analysis leading from Equation 4.1 to Equation 4.11 is only applicable for the range of R_ρ^o over which double diffusion is observed. In the limits $R_\rho^o \to 0$ and $R_\rho^o \to \infty$, the analysis is no longer meaningful because double diffusion is replaced by other transport processes.

One further test of the relation proposed should be possible from our observations by calculating the heat flux implied by Equation 4.9 in the higher section of double diffusive layering between 301–309 m (Figure 3.2). In order to be consistent, the relation would need to calculate a heat flux that is roughly the same as the steady state heat flux estimated in the lower staircase. However, in practice this is difficult because the double diffusive region between 301-309 m consists of only a small number of layers. Because the vertical height of the staircase is only a few times larger than the scale-height of a layer, the background temperature gradient has relatively large transition zones at the edges of the double diffusive zone. Furthermore, the layers are not observed consistently across the basin, making it difficult to determine where the double diffusive instability is present. Using values

$$\frac{\partial T}{\partial z} = 0.0042\,^\circ\mathrm{C/m} \quad \text{and} \quad R_\rho^o = 2.75 \tag{4.12}$$

averaged over the staircase between 302–307 m, Equation 4.9 calculates a heat flux of 26 $\mathrm{mW/m^2}$. While this value is remarkably close to the heat flux estimated in the lower staircase, we emphasize that it should be viewed with caution and only as a rough estimate because of the inherent difficulty of defining the background temperature gradient.

Many open questions remain, but the obvious next step in pursuing this topic would be a comparison with datasets from other locations such as Lake Kivu and the Arctic. If the relationship given by Equation 4.9 holds for observations of double diffusion in these locations, there would be sufficient evidence to encourage further observational and laboratory based work. The meaning of the proportionality constant m remains a mystery, and it is unclear from one dataset whether it is dependent only on the physical properties of the lake or seawater solution (that is τ and Pr) or also on other parameters. However, our observations suggest that m should be independent of R_ρ and Ra.

4.5 Interface Characteristics - Temperature Gradient

The discrepancy between the interfacial temperature gradient we calculate and the temperature gradient that should be expected from molecular diffusion (Section 3.3) can be explained in two ways. The first explanation is that ∇t as we define it does not accurately represent the maximum gradient in the interface. Because we calculate ∇t from the bulk interface parameters Δt and h_T (rather than trying to estimate the maximum gradient somewhere within the interface directly), we in fact average the gradient over the entire interface.

Using this approach, it is likely that we underestimate the maximum interfacial gradient since there may be boundary layers at the edges of the interface. However, the boundary layers at the edges of the interface would need to comprise a sizeable proportion of the total interface height in order for us to underestimate the maximum gradient by more than a factor of two. If we take the measured value of δh to be representative of the size of the boundary layer, then on average the two boundary layers (one on either side of the interface) together comprise only about 9% of the total interface height. A boundary layer of this size would likewise bias our gradient calculation by approximately 9%. Visually comparing the calculated gradient to the observed shape of the interface verifies that the boundary layers are often small, that the layer-finding algorithm correctly identifies the layer/interface boundaries, and that the gradient calculated from bulk interfacial parameters is largely representative of the actual interfacial gradient (Figure 4.3). While there may yet be a small portion within the interface in which the gradient is large enough to support the steady state flux by molecular diffusion (a diffusive "core"), it would need to be substantially smaller than the overall size of the interface to be consistent with our observations.

In addition, invoking the argument that our method of calculating ∇t dramatically underestimates the maximum interfacial gradient does not account for the observed correlation between the strength of the gradient and the stability of the interface. We find that as the interface becomes more stable with increasing R_ρ, the strength of the mean temperature gradient in the interface approaches that which would be expected from molecular diffusion (Figure 3.9). This leads to the second explanation which can be invoked to explain the difference between the expected and observed interfacial gradients.

Lab experiments by Marmorino and Caldwell (1976) find that, while for high values of R_ρ the measured heat flux across a double diffusive interface is that which would be expected from molecular diffusion, at low values of R_ρ the measured heat flux becomes larger than the diffusive flux. The authors quote that at $R_\rho = 2$ the net vertical heat flux is 2.5 times the diffusive flux. Likewise, the lower-than-expected interfacial temperature gradient we calculate in Powell Lake can be explained by allowing for interfacial transport that is not strictly due to molecular diffusion. Under this interpretation, at low density ratios

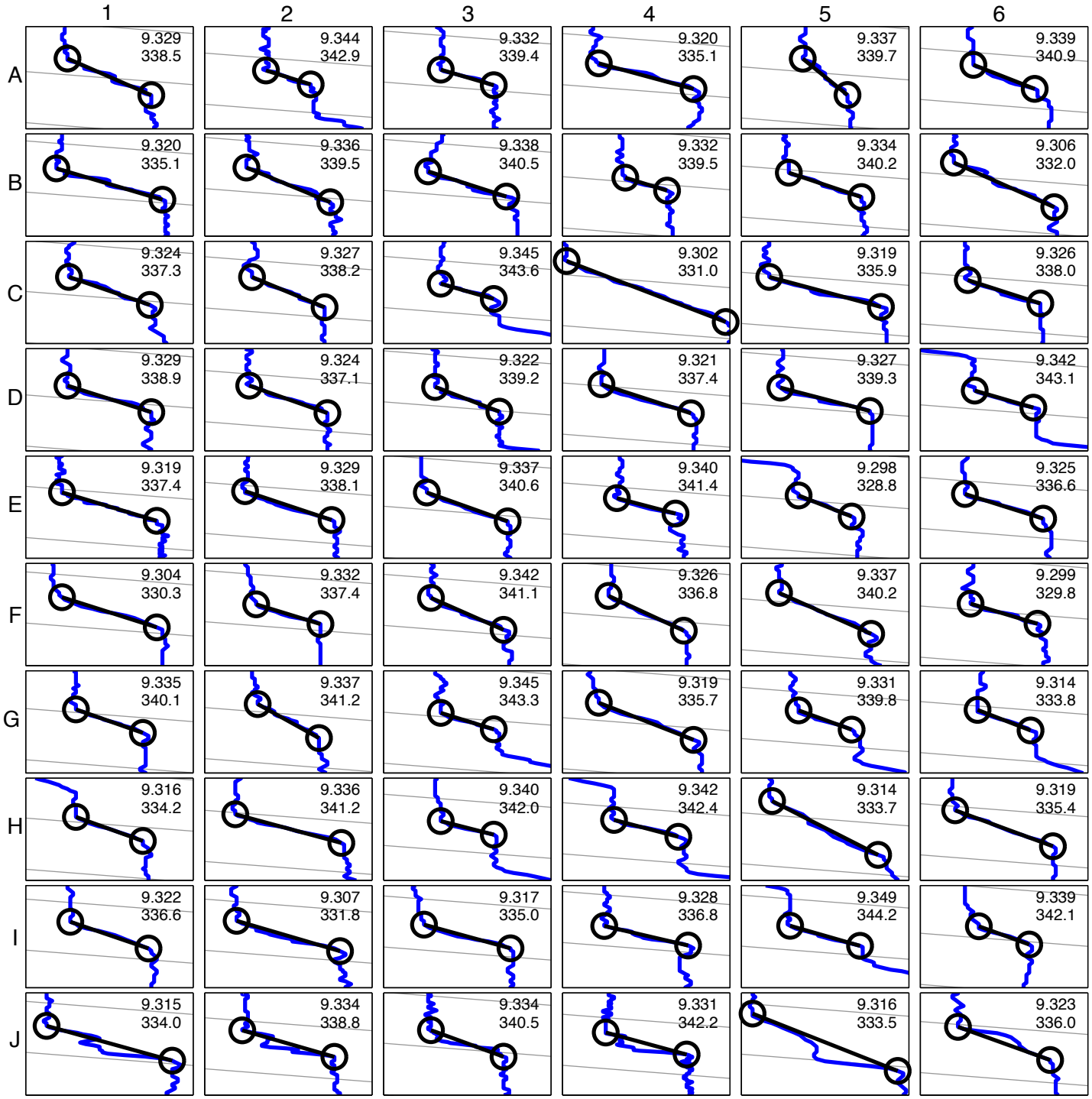

Figure 4.3 – Sixty examples of the double diffusive interface in which the calculated temperature gradient (black line) is lower than the expected steady state gradient of 0.047 °C/m (thin grey lines in the background). The actual interface measurements are given in blue and the edges of the interface as chosen by our algorithm are shown by open circles. In Panels A1-I6, the algorithm accurately calculates the observed gradient. In Panels J1-J6, the algorithm underestimates the interfacial gradient. The vertical range on all panels is one meter, and the horizontal range on all panels is 0.006 °C. The lower bound temperature (°C) and lower bound depth (m) are given in the top right corner of each panel.

slightly more than half of the interfacial transport is due to a secondary process active in the interface. This is evident because the observed gradient is slightly less than half the value dictated by molecular diffusion. Molecular diffusion remains important, but at low density ratio, it is no longer the sole mechanism transporting heat from one layer to the next. Thus our results are in excellent agreement with those of Marmorino and Caldwell (1976), and to our knowledge, there have been no laboratory experiments that contradict these findings.

The above interpretation naturally explains the strong linear relationship between ∇t and R_ρ depicted in Figure 3.9. As the interface becomes less stable with decreasing R_ρ, an increasingly higher proportion of the interfacial transport is due to mixing processes within the interface or direct interaction between successive layers. Conversely, as the interface becomes more stable with increasing R_ρ, convecting layers cease to interact with each other directly and transport becomes dominated by molecular diffusion. Though this result is contradictory to the practice of estimating double diffusive fluxes by assuming pure molecular diffusion across the interface, it should not be a surprising result that as the interface becomes less stable, entrainment from adjacent convecting layers across this relatively thin density barrier begins to become important and affect the dynamics of the interface. Previous studies have considered that rising and falling convective plumes within mixed layers may entrain heat from one layer to the next as they push or shear against the interface (Padman and Dillon, 1987; Schmid et al., 2004, 2010). However, ours is the first study to provide observational evidence from a natural setting that this may indeed be the case.

Keeping in mind the above discussion, there are cases in which our layer-finding algorithm has difficulty estimating the interfacial gradient correctly, and in these scenarios it will tend to underestimate rather than overestimate the actual gradient in the interface. A few examples of this are given in Figure 4.3, Panels J1–J6. Usually the algorithm will obviously underestimate the actual gradient only if the observed interface is disturbed or asymmetric. We have chosen to include these interfaces in our analysis because there is no basis to conclude that a dynamic interface will always be well described by an idealized function such as a hyperbolic tangent or an error function. In fact, if there is a secondary transport process in the interface, we would expect to see interface shapes that appear disturbed and which do not follow an idealized shape.

While it may not be possible to say definitively which of the two interpretations discussed above is correct, it is certain from our observations that the mean vertical heat flux cannot in general be calculated accurately from the bulk properties of the interface. This finding should be incorporated into future studies where double diffusive fluxes are estimated from direct interface measurements.

4.6 Interface Characteristics - Relative Thickness

Microstructure observations of the double diffusive interface in salinity are extremely scarce or undocumented, so we are unable to perform comparisons with other studies. However, based on a model in which the diffusion rates of heat and salt determine the relative sizes of the temperature and salinity interfaces, it is surprising that the temperature interfaces we measure are only marginally larger than the salinity interfaces (Figure 3.6b). If the interfaces in temperature and salinity grow by molecular diffusion, scaling the one-dimensional diffusion equation suggests that the interface heights scale as

$$h_T = \sqrt{\kappa_T \, t^+} \tag{4.13a}$$

$$h_S = \sqrt{\kappa_S \, t^+} \tag{4.13b}$$

where t^+ is the time scale of the diffusion. The ratio of the two interface heights is then independent of time and given by

$$r_h = \frac{h_T}{h_S} = \sqrt{\frac{\kappa_T}{\kappa_S}} \approx 10 \tag{4.14}$$

As outlined in Section 1.4, the differing rates at which the two interfaces grow is thought to result in unstable boundary layers on either side of the interface which eventually break away as convective plumes. The difference in height δh of the temperature and salinity interfaces shown Figure 3.6b is then a measure of the boundary layer size. Specifically, it is the mean combined height of the boundary layers above and below the interface.

Using the observed mean interface heights of $h_T = 18$ cm and $h_T = 17$ cm, we find that the interface height ratio is $r_h = 1.1$ in Powell Lake. This is inconsistent with the prediction from Equation 4.14. Though the value $r_h \approx 10$ is an upper bound because boundary layers may be eroded by convection in the adjacent mixed layers, the extremely low value of r_h that we observe may indicate that the size of the interface and adjacent boundary layers is not controlled solely by molecular diffusion.

A possible explanation to resolve the discrepancy between the expected and observed interface heights is that there is a semi-permanent background interface of finite thickness η which is approximately constant (Figure 4.4a). Around this background interface, relatively small boundary layers grow because of molecular diffusion, and these small boundary layers break away when they become unstable leaving the background interface unchanged. In this scenario, the scaling 4.14 for the relative interface heights is replaced by one for the relative boundary layer heights:

$$r_b = \frac{h_T - \eta}{h_S - \eta} = \sqrt{\frac{\kappa_T}{\kappa_S}} \approx 10 \tag{4.15}$$

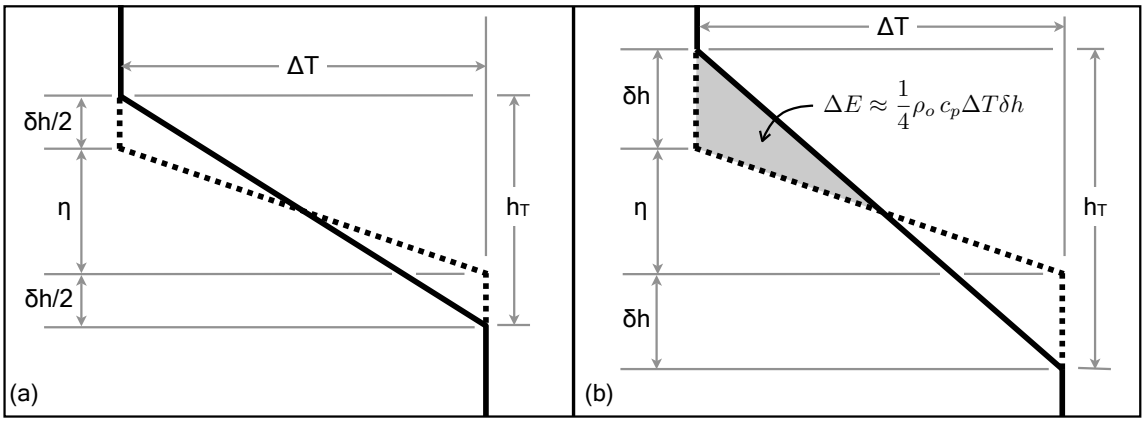

Figure 4.4 – (a) A simplified model of the temperature interface based on our observations. There is a semi-permanent background interface of approximately constant height η, shown by the dashed line. Around this background interface, boundary layers grow on either side, which on average have a height of $\delta h/2$. The average observed interface (thick black line) then has a height $h_T = \eta + \delta h$. (b) A typical boundary layer will grow to a height δh before an instability sets in and it breaks away from the interface. The thermal energy ΔE per unit area stored in the boundary layer at this time is proportional to the area of the grey shaded triangle. In both panels the size of the boundary layer relative to the background interface is exagerated.

where r_b is the ratio of the diffusive boundary layers in temperature and salinity. In practice, η will be only slightly smaller than h_S, and from our measurements the two would be indistinguishable. For example, if $h_T = 18.0$ cm and $h_S = 17.0$ cm, then a value of $r_b = 10$ would require that $\eta = 16.8$ cm. In the explanation given here, it remains unclear what determines the size of η and this could be the subject of future study, but we will at least show that the model described here is consistent with the estimated heat flux of 27 mW/m^2.

Based on the estimated heat flux and boundary layers that thicken due to molecular diffusion, it is possible to infer a scale height for δh. To begin, consider an interface whose boundary layers have recently been eroded; the interface now has a height $h_T = h_S = \eta$. Boundary layers will subsequently begin to form on either side of the interface as the temperature interface grows more quickly than the salinity interface. We observe that the combined height of the two boundary layers is on average δh; therefore, the temperature interface on average has a height $h_T = \eta + \delta h$. If this is the observed average height, then a typical temperature interface will grow to a size $h_T = \eta + 2\,\delta h$ before instability separates the boundary layer from the interface (Figure 4.4b). The factor of 2 arises because the instability should occur at the maximum boundary layer height which will be approximately twice the mean observed boundary layer height averaged over time. Meanwhile, for simplicity we approximate the salinity interface as constant so that $h_S = \eta$ always.

Now it is possible to estimate the thermal energy ΔE accumulating in one of the growing

boundary layers by integrating the temperature profile over the boundary layer. ΔE is proportional to the area of the triangle formed in T–z space by the boundary layer (Figure 4.4b). This is independent of η. Approximating the temperature profile in the interface as linear, the area A of the triangle is $\frac{1}{2}(\delta h)(\frac{1}{2}\Delta T)$ and so

$$\Delta E = \rho_o \, c_p \, A \approx \frac{1}{4} \rho_o \, c_p \Delta T \delta h \tag{4.16}$$

The energy accumulated in the interface is also equal to the heat flux into the interface multiplied by the time scale t^+ of the diffusion:

$$\Delta E \approx F_H \, t^+ \tag{4.17}$$

Substituting (4.17) into (4.16) and rearranging for δh gives

$$\delta h \approx \frac{4 F_H t^+}{\rho_o c_p \Delta T} \tag{4.18}$$

The time scale, from the one-dimensional diffusion equation, is

$$t^+ \approx \delta h^2 / k_T \tag{4.19}$$

and thus

$$\delta h \approx \frac{\rho_o c_p \kappa_T \Delta T}{4 F_H} \tag{4.20}$$

Substituting values from Equation 3.4 along with $\Delta T = 4.0 \times 10^{-3}$ °C and $F_H = 27$ mW/m^2 yields $\delta h \approx 2$ cm. For a simple scaling argument, this is remarkably consistent with our observation that $\delta h = 1.5$ cm.

As a consequence of the discussion outlined in this Section, we conclude that the overall size of the double diffusive interfaces we observe does not appear to be determined by molecular diffusion alone. This is evidenced by the extremely low observed value of r_h. Rather, it could be that the interface has a semi-permanent background structure of finite size with diffusive boundary layers that are small compared to the overall interface. It is not evident how the size of the background structure of the interface is determined, but it is clear that scaling the size of the entire interface based solely on the relative diffusion rates of heat and salt (Equation 4.14) is not the correct approach for describing the interfaces we observe. This conclusion can be taken in conjunction with those of Section 4.5 to further indicate that the bulk properties of the interface are not necessarily controlled only by molecular diffusion.

Chapter 5

Conclusion

This study reports on observations of double diffusive layering in Powell Lake, British Columbia, which contains a 60 m geothermally heated, anoxic layer of relic seawater dating back to the most recent deglaciation. Double diffusion is isolated from turbulent and convective transport mechanisms in the deep, quiescent water, making Powell Lake a unique and ideal natural laboratory in which to study the phenomenon. We have obtained basin-wide fine-scale measurements of temperature and salinity within the double diffusive staircase, yielding a robust set of layer and interface statistics. Convecting layers tend to be coherent on the basin scale giving them an aspect ratio as large as 10^4. They tend to have a height of about 0.5–0.9 m and the dividing interfaces between layers tend to be about 0.1–0.2 m high.

Powell Lake is a unique system in which to study double diffusion because precise, independent estimates of the steady state vertical heat flux through the staircase are available. These estimates allow us to test the accuracy of current double diffusive flux parameterizations with unprecidented precision. We find that parameterized heat fluxes are accurate to within a factor of 2, but deviate from the steady state flux in a systematic manner. We find that the underlying power law scaling $Nu \propto Ra^n$ does not represent the trend in our observations very well. Consequently, we propose a new scaling of the form $Nu \propto R_\rho^{-1}$ which has apparently not been examined before, but which much better matches our observations. We also outline that a scaling of this form has theoretical advantages over the traditional scaling that leads to the current 4/3 flux parameterizations.

The combination of fine scale measurements in temperature and conductivity together with a known vertical heat flux allows us to test the properties of the interface between mixed double diffusive layers. We find that for low density ratio (approximately $R_\rho < 4$) the average temperature gradient in the interface is less than half that needed to account for the steady state heat flux by molecular diffusion alone. From our observations it cannot be

ruled out that there is a thin diffusive core somewhere within the interface where molecular diffusion consistently dominates; however, taking the interface as a whole, it appears that another transport mechanism of rougly the same strength as molecular diffusion contributes to the interfacial heat flux. We also find that the strength of the interfacial temperature gradient correlates to the observed density ratio, which implies that if there is a secondary transport mechanism through the interface, this mechanism becomes increasingly important as the density stratification across the interface becomes weaker with decreasing R_ρ.

Furthermore, observations of the relative interface thicknesses h_T and h_S indicate that molecular diffusion alone does not set the size of the interface. This is evident because the ratio of interface thicknesses r_h is close to unity. The observed value of r_h can be explained by developing a model for the interface where the boundary layers in which the instability forms due to molecular diffusion comprise only a small proportion of the total observed interface height. The mechanism that then determines the height of the background interface is independent of the instability but remains unexplained. However, we show by a simple scaling argument that the observed difference δh between the temperature and salinity interfaces is consistent with the estimated steady state heat flux.

Bibliography

K. E. Barner and G. R. Arce. Order-statistic filtering and smoothing of time-series: part ii. *Handbook of statistics*, 17:555–602, 1998.

S. W. Bruenn and T. Dineva. The role of doubly diffusive instabilities in the core-collapse supernova mechanism. *The Astrophysical Journal Letters*, 458(2):L71, 1996.

E. Carmack, W. Williams, S. Zimmermann, and F. McLaughlin. The Arctic Ocean warms from below. *Geophysical Research Letters*, 39(7):L07604, 2012.

J. R. Carpenter and M.-L. Timmermans. Temperature steps in salty seas. *Physics Today*, 65:66–67, 2012.

J. R. Carpenter, T. Sommer, and A. Wüest. Stability of a double-diffusive interface in the diffusive convection regime. *Journal of Physical Oceanography*, 42:840–854, 2012.

B. Castaing, G. Gunaratne, L. Kadanoff, A. Libchaber, and F. Heslot. Scaling of hard thermal turbulence in rayleigh-bénard convection. *Journal of Fluid Mechanics*, 204(1): 1–30, 1989.

C. Chen and D. Johnson. Double-diffusive convection: A report on an engineering foundation conference. *Journal of Fluid Mechanics*, 138:405–16, 1984.

W. S. Cleveland. *Visualizing Data*. Hobart Press, 1993. ISBN 0963488406.

P. Crapper. Measurements across a diffusive interface. *Deep Sea Research and Oceanographic Abstracts*, 22(8):537 – 545, 1975.

K. Fedorov. Layer thicknesses and effective diffusivities in diffusive thermohaline convection in the ocean. *Small-scale turbulence and mixing in the ocean. Elsevier*, pages 471–479, 1988.

S. Grossmann and D. Lohse. Thermal convection for large Prandtl numbers. *Physical Review Letters*, 86(15):3316–3319, 2001.

F. Heslot, B. Castaing, and A. Libchaber. Transitions to turbulence in helium gas. *Physical Review A*, 36:5870–5873, Dec 1987.

R. D. Hyndman. Heat flow measurements in the inlets of southwestern British Columbia. *Journal of Geophysical Research*, 81(2):337–349, 1976.

IOC, SCOR, and IAPSO. *The international thermodynamic equation of seawater - 2010: Calculation and use of thermodynamic properties*. Manual and Guides No. 56.

Intergovernmental Oceanographic Commission, UNESCO (English), 2010. Available from http://www.TEOS-10.org.

T. J. McDougall. Greenland Sea bottom water formation: A balance between advection and double-diffusion. *Deep Sea Research Part A. Oceanographic Research Papers*, 30 (11):1109–1117, 1983.

D. E. Kelley. Effective diffusivities within oceanic thermohaline staircases. *Journal of Geophysical Research*, 89(10):484–10, 1984.

D. E. Kelley. Fluxes through diffusive staircases: A new formulation. *Journal of Geophysical Research*, 95(3365):71, 1990.

D. E. Kelley, H. J. S. Fernando, A. E. Gargett, J. Tanny, and E. Özsoy. The diffusive regim of double-diffusive convection. *Progress in Oceanography*, 56:461–468, 2003.

E. Kunze. A review of oceanic salt-fingering theory. *Progress in Oceanography*, 56(34):399 – 417, 2003.

P. F. Linden and T. G. L. Shirtcliffe. The diffusive interface in double-diffusive convection. *Journal of Fluid Mechanics*, 87(part 3):417–432, 1978.

G. O. Marmorino and D. R. Caldwell. Heat and salt transport through a diffusive thermohaline interface. *Deep Sea Research and Oceanographic Abstracts*, 23(1):59 – 67, 1976.

W. H. Mathews. Bathymetry of Powell Lake, British Columbia. Technical Report 13, Institute of Oceanography, University of British Columbia, 1962.

W. H. Mathews, J. Fyles, and H. Nasmith. Postglacial crustal movements in southwestern British Columbia and adjacent Washington State. *Canadian Journal of Earth Sciences*, 7(2):690–702, 1970.

W. J. Merryfield. Hydrodynamics of semiconvection. *The Astrophysical Journal*, 444: 318–337, 1995.

W. J. Merryfield. Origin of thermohaline staircases. *Journal of physical oceanography*, 30 (5):1046–1068, 2000.

T. Newell. Characteristics of double-diffusive interface at high density stability ratios. *Journal of Fluid Mechanics*, 149:385–401, 1984.

T. Noguchi and H. Niino. Multi-layered diffusive convection. Part 1. Spontaneous layer formation. *Journal of Fluid Mechanics*, 651:443–464, 2010a.

T. Noguchi and H. Niino. Multi-layered diffusive convection. Part 2. Dynamics of layer evolution. *Journal of Fluid Mechanics*, 651:465–481, 2010b.

T. R. Osborn. Temperature microstructure in Powell Lake. *Journal of Physical Oceanography*, 3:302–307, 1973.

L. Padman and T. M. Dillon. Vertical heat fluxes through the Beaufort Sea thermohaline staircase. *Journal of Geophysical Research: Oceans*, 92(C10):10799–10806, 1987.

L. Padman and T. M. Dillon. Thermal microstructure and internal waves in the Canada Basin diffusive staircase. *Deep Sea Research Part A. Oceanographic Research Papers*, 36 (4):531 – 542, 1989.

K. Perry and T. Pedersen. Sulphur speciation and pyrite formation in meromictic ex-fjords. *Geochimica et cosmochimica acta*, 57(18):4405–4418, 1993.

I. Polyakov, A. Pnyushkov, R. Rember, V. Ivanov, Y. Lenn, L. Padman, and E. Carmack. Mooring-based observations of double-diffusive staircases over the Laptev Sea slope. *Journal of Physical Oceanography*, 42(1):95–109, 2012.

T. Radko. A mechanism for layer formation in a double-diffusive fluid. *Journal of Fluid Mechanics*, 497:365–380, 2003.

E. Rosenblum, P. Garaud, A. Traxler, and S. Stellmach. Turbulent mixing and layer formation in double-diffusive convection: three-dimensional numerical simulations and theory. *The Astrophysical Journal*, 731(1):66, 2011.

B. Ruddick and A. E. Gargett. Oceanic double-infusion: introduction. *Progress in Oceanography*, 56(34):381 – 393, 2003.

B. Rudels, E. P. Jones, U. Schauer, and P. Eriksson. Atlantic sources of the Arctic Ocean surface and halocline waters. *Polar Research*, 23(2):181–208, 2004.

B. Sanderson, K. Perry, and T. Pedersen. Vertical diffusion in meromictic Powell Lake, British Columbia. *Journal of Geophysical Research*, 91:7647–7655, 1986.

M. Schmid, A. Lorke, C. Dinkel, G. Tanyileke, and A. Wüest. Double-diffusive convection in Lake Nyos, Cameroon. *Deep Sea Research I*, 51:1097–1111, 2004.

M. Schmid, M. Busbridge, and A. Wüest. Double-diffusive convection in Lake Kivu. *Limnology and Oceanography*, 55:225–238, 2010.

R. Schmitt. Double diffusion in oceanography. *Annual Review of Fluid Mechanics*, 26(1): 255–285, 1994.

R. Schmitt. Observational and laboratory insights into salt finger convection. *Progress in Oceanography*, 56(34):419 – 433, 2003.

R. Schmitt, H. Perkins, J. Boyd, and M. Stalcup. C-salt: An investigation of the thermohaline staircase in the western tropical North Atlantic. *Deep Sea Research Part A. Oceanographic Research Papers*, 34(10):1655 – 1665, 1987.

M. H. Sharqawy, J. H. Lienhard, and S. M. Zubair. Thermophysical properties of seawater: A review of existing correlations and data. *Desalination and Water Treatment*, 16(1-3):354–380, 2010.

H. Sigurdsson, J. Devine, F. Tchua, F. Presser, M. Pringle, and W. Evans. Origin of the lethal gas burst from Lake Monoun, Cameroun. *Journal of Volcanology and Geothermal Research*, 31(1):1–16, 1987.

G. E. Sigvaldason. International conference on Lake Nyos disaster, Yaoundé, Cameroon

16–20 March, 1987: Conclusions and recommendations. *Journal of Volcanology and Geothermal Research*, 39(2–3):97–107, 1989.

T. Sommer and A. Wüest. Double-diffusive convection in Lake Kivu. 2013. In preparation.

M. E. Stern. The salt-fountain and thermohaline convection. *Tellus*, 12(2):172–175, 1960.

H. Stommel. An oceanographical curiosity: the perpetual salt fountain. *Deep Sea Research Part II: Topical Studies in Oceanography*, 3:152–153, 1956.

M.-L. Timmermans, J. Toole, R. Krishfield, and P. Winsor. Ice-Tethered Profiler observations of the double-diffusive staircase in the Canada Basin. *Journal of Geophysical Research*, 113, 2008.

J. S. Turner. The coupled turbulent transports of salt and and heat across a sharp density interface. *International Journal of Heat and Mass Transfer*, 8(5):759–767, 1965.

J. S. Turner. *Buoyancy effects in fluids*. Cambridge University Press, New York, 1973.

P. M. Williams, W. H. Mathews, and G. L. Pickard. A lake in British Columbia containing old sea-water. *Nature*, 191:830–832, 1961.